INTERNATIONAL SCIENTIFIC JOURNAL

MATHEMATICAL MODELING

YEAR Y, ISSUE 4/2021
ISSN (PRINT) 2535-0986
ISSN (WEB) 2603-2929

Published by
SCIENTIFIC-TECHNICAL UNION of MECHANICAL ENGINEERING - INDUSTRY 4.0
Sofia, BULGARIA

INTERNATIONAL EDITORIAL BOARD

EDITOR I CHIEF	
Prof. ANDREY FIRSOV Peter the Great St.Petersburg Polytechnic University	RU

Members:		
Abilmazhin Adamov, Prof.	L.N.Gumilyov Eurasian National University	KZ
Alexander Guts, Prof.	Omsk State University	RU
Alexei Zhabko, Prof.	Saint Petersburg State University	RU
Andrey Markov, Prof.	Baltic State Technical University	RU
Andrii Matviichuk, Prof.	Kyiv National Economics University	UA
Andrzej Nowakowski, Prof.	University of Lodz	PL
Anton Makarov, Dr.	Saint Petersburg State University	RU
Armands Gricans, Assoc. Prof.	Daugavpils University	LV
Artūras Dubickas, Prof.	Vilnius University	LT
Avinir Makarov, Prof.	Saint Petersburg State University of Industrial Technologies and Design	RU
Christo Boyadjiev, Prof.	Institute of Chemical Engineering, BAS	BG
Daniela Marinova, Dssoc. Prof.	Technical University of Sofia	BG
Dimitrios Poulakis, Prof.	Aristotle University of Thessaloniki	GR
Evgeniy Smirnov, Assoc. Prof.	Volgograd State Technical University	RU
Galia Angelova, Prof. DSc,	Bulgarian Academy of Science	BG
Giovanni Borgioli, Assoc. Prof.	University of Florence	IT
Haskiz Coskun, Prof.	Karadeniz Technical University of Trabzon	TR
Idilia Bachkova, Prof.	University of Chemical Technology and Metallurgy	BG
Igor Anufriev, Assoc. Prof.	Peter the Great St.Petersburg Polytechnic University	RU
Irena Stojkovska, Prof.	Ss. Cyril and Methodius University in Skopje	MK
Ivana Štajner-Papuga, Prof.	University of Novi Sad	RS
Kanagat Aldazharov, Assoc. Prof.	Kazakh Economics University	KZ
Karl Kunisch, Prof.	University of Graz	AT
Mahomed Agamirza ogly Dunyamalyev, Prof.	Azerbaijan Technical University	AZ
Marius Giuclea, Prof.	The Bucharest University of Economics Studies	RO
Mihail Okrepilov, Prof.	D.I. Mendeleyev Institute for Metrology (VNIIM)	RU
Milena Racheva, Assoc. Prof.	Technical University of Gabrovo	BG
Mohamed Kara, Dr.	Ferhat Abbas Sétif 1 University	DZ
Mohamed Taher El-mayah, Prof	MTI University	EG
Neli Dimitrova, Prof.	Institute of Mathematics and Informatics, BAS	BG
Nina Bijedic, Prof.	Dzemal Bijedic University of Mostar	BA
Oleg Obradović, Prof.	University of Montenegro	ME
Olga Pritomanova, Assoc. Prof.	Oles Honchar Dnipropetrovsk National University	UA
Özkan Öcalan, Prof.	Akdeniz University of Antalya	TR
Paşc Găvruţă, Prof.	Politehnic University of Timisoara	RO
Pavel Satrapa, Assoc. Prof.	Technical University of Liberec	CZ
Pavel Tvrdík, Prof.	Czech Technical University in Prague	CZ
Pavlina Yordanova, Assoc. Prof.	Shumen University	BG
Petr Trusov, Prof.	Perm State Technical University	RU
Rannveig Björnsdóttir, Prof.	University of Akureyri	IS
Roumen Anguelov, Prof.	University of Pretoria	ZA
Sándor Szabó, Dr. Prof.	University of Pécs	HU
Sashko Martinovski, Assoc. Prof.	St. Kliment Ohridski University of Bitola	MK
Sergey Bosnyakov, Prof.	Moscow Institute of Physics and Technology	RU
Sergey Kshevetskii, Prof.	Immanuel Kant Baltic Federal University	RU
Snejana Hristova, Prof.	University of Plovdiv	BG
Svetlana Lebed, Assoc. Prof.	Brest State Technical University	BY
Tomasz Szarek, Prof.	University of Gdansk	PL
Valeriy Serov, Prof.	University of Oulu	FI
Vasily Maximov, Prof.	Saint Petersburg State University of Industrial Technologies and Design	RU
Ventsi Rumchev, Prof.	Curtin University, Perth	AU
Veronika Stoffová, Prof.	University of Trnava	SK
Veselka Pavlova, Prof.	University of National and World Economy	BG
Viorica Sudacevschi, Assoc. Prof.	Technical University of Moldova	MD
Vladimir Janković, Prof.	University of Belgrade	RS
Vladislav Holodnov, Prof.	Saint Petersburg State Institute of Technology	RU
Vyacheslav Demidov, Prof.	Saint Petersburg State University of Industrial Technologies and Design	RU
Yordan Yordanov, Assoc. Prof.	University of Sofia	BG
Yuriy Kuznetsov, Prof.	Nizhny Novgorod State University	RU
Zdenka Kolar - Begović, Prof.	University of Osijek	HR

INTERNATIONAL SCIENTIFIC JOURNAL

MATHEMATICAL MODELING

PUBLISHER:

SCIENTIFIC TECHNICAL UNION OF MECHANICAL ENGINEERING "INDUSTRY 4.0"

108, Rakovski Str., 1000 Sofia, Bulgaria
tel. (+359 2) 987 72 90,
tel./fax (+359 2) 986 22 40**,**
office@stumejournals.com
www.stumejournals.com

ISSN (PRINT) 2535-0986
ISSN (WEB) 2603-2929
YEAR V, ISSUE 4 / 2021

EDITOR IN CHIEF:

Prof. D.Sc. ANDREY FIRSOV
Peter the Great St.Petersburg Polytechnic University, Russia

CONTENTS

THEORETICAL FOUNDATIONS AND SPECIFICITY OF MATHEMATICAL MODELLING

Formulation of axisymmetric boundary value problems of the linear theory of elasticity for canonical bodies in harmonic potentials
Viktor Pabyrivskyi, Nelya Pabyrivska, Galyna Beregova 116

Consistent Presentation of the Beam Deflection Theory Including Shear Correction
Rumen Krastev 120

MATHEMATICAL MODELLING OF TECHNOLOGICAL PROCESSES AND SYSTEMS

Application of artificial locust swarm routing algorithm for VFR flights planning
Vladyslav Alieksieiev, Halyna Ivasyk, Ivanna Andrusiak 124

Automated system of getting meter readings in the sphere of communal services
Volodymyr Hladun, Bohdan Liubinsky, Petro Topylko 128

A new Approach to Modeling and Simulation of Industrial Processes
Christo Boyadjiev 130

Multicriterial optimization strategies for electron beam grafting of corn starch
Lilyana Koleva, Zlatina Petrova, Elena Koleva, Mirela Braşoveanu, Monica R. Nemţanu, Georgi Kolev 133

Implementation of simulation tools in optimization of traffic flows – case study City of Zagreb
Nikola Kožul, Luka Novačko 136

Numerical modeling of impact interaction between an active element and a deformable barrier
Krumov Angel, Simeonova Antoaneta 139

MATHEMATICAL MODELLING OF SOCIO-ECONOMIC PROCESSES AND SYSTEMS

Application of artificial neural networks for prediction of business indicators
Petar Halachev 141

Decarbonizing Russia: leapfrogging from fossil fuel to hydrogen
Vladimir Potashnikov, Alexander Golub, Michael Brody, Oleg Lugovoy 145

Formulation of axisymmetric boundary value problems of the linear theory of elasticity for canonical bodies in harmonic potentials

Viktor Pabyrivskyi[1,2], Nelya Pabyrivska[1,3], Galyna Beregova[1,4],
[1]Lviv Polytechnic National University, Lviv, Ukraine
[2]Victor.V.Pabyrivskyi@lpnu.ua, https://orcid.org/ 0000-0002-6071-3817
[3] Nelia.V. Pabyrivska@lpnu.ua, https://orcid.org/0000-0003-4631-0189
[4] Halyna.I.Berehova@lpnu.ua, https://orcid.org/0000-0002-4535-2849

Abstract: *The paper is based on the representation of the fundamental solution of the linear elasticity theory of the mechanics of a deformable solid in the J. Dougall's form through spatial harmonic functions. The axisymmetric problem of the elasticity theory in a cylindrical coordinate system for bodies bounded by a canonical surface is formulated. As a case, the boundary value problem of pure torsion is formulated and the elastic characteristics and structure of the corresponding external loads on the side surface of a given isotropic elastic body in the above-mentioned harmonic potentials are presented. This approach makes it possible to obtain and extend the set of exact analytical solutions of boundary value problems of the spatial elasticity theory and is the theoretical basis for calculating the strength parameters of mechanical systems.*

Keywords*: THREE-DIMENSIONAL THEORY OF ELASTICITY; BOUNDARY VALUE PROBLEM; DISPLACEMENT VECTOR; STRESS TENSOR; DEFORMATION TENSOR; BASIC SOLUTIONS; HARMONIC FUNCTION.*

1. Introduction

An important area of research in the mechanics of a deformed body is the spatial problems of the elasticity theory. The relevance of basic research on this topic is characterized by the fact that in most cases, the stress-strain state of the body is 3-dimensional. Today, both numerical and analytical approaches for solving boundary value problems of the spatial elasticity theory have been built.

Methods of solving the problems of static elasticity known from the literature are based on solutions of homogeneous equilibrium equations in displacements using harmonic and biharmonic functions. Such solutions have been proposed, in particular, by W.Kelvin, P.Tait [1] and M.Boussinesq [2]. B.Galerkin [3] presented the general solution of the equations of elastic equilibrium of an isotropic body through three biharmonic functions. In the works of P.F.Papkovych [4] and H.Neuber [5] the form of the general solution was given through vector and scalar harmonic functions. Optimization of this representation only through three spatial harmonic functions have been published in scientific papers [6,7]. This solution representation has become the basis for solving the three-dimensional boundary value problem of the theory of elasticity for bodies of rotation [8].

Given the complexity of constructing solutions of boundary value problems of the elasticity theory in three-dimensional space, assumptions are often made about the structure of deformation of elastic bodies. The monographs of A.I. Lurie [9] and J.N.Goodier, S.P.Timoshenko [10] investigates general methods for solving the basic equations of equilibrium of an isotropic and anisotropic body, which is of great importance for the development of research on spatial problems of the elasticity theory.

J.Dougall [11] was one of the first to propose an approach to construct a general solution to the problem of the theory of elasticity for a cylinder in three-dimensional space. In [12], the authors used two representations of Dugall through harmonic functions to construct a general solution of the problem of the elasticity theory for a continuous finite cylinder, which allows to satisfy the boundary conditions both at the ends and on the side surface of the cylinder.

Representation of the Dugall's solution through three spatial harmonic scalar functions was used as a basis for formulating the boundary value problem of torsion for bodies bounded by a canonical surface, which will expand the set of exact analytical solutions and become a theoretical basis for calculating the strength parameters of mechanical systems.

2. Formulation of the problem of the linear elasticity theory for a body bounded by a canonical surface

An isotropic elastic body X in three-dimensional space is considered, which is bounded by the surface ∂X, which is described by the canonical curve $f(r,\theta,z)=0$. (Fig. 1).

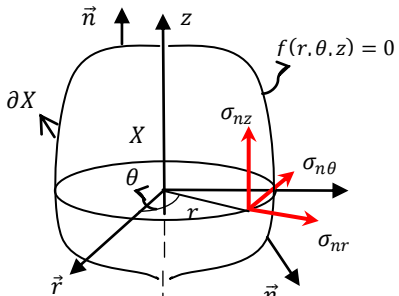


Fig. 1 *Elastic isotropic body bounded by a canonical surface*

The body is under the action of a stationary force load, which is applied to the lateral surface of the body ∂X.

The first boundary value problem of the linear elasticity theory for a given elastic isotropic body in the absence of bulk forces in a cylindrical coordinate system (r,θ,z) has the form.

– equilibrium equation:

$$\frac{\partial\sigma_{rr}}{\partial r}+\frac{1}{r}\frac{\partial\sigma_{r\theta}}{\partial\theta}+\frac{\partial\sigma_{rz}}{\partial z}+\frac{\sigma_{rr}-\sigma_{\theta\theta}}{r}=0,$$

$$\frac{\partial\sigma_{rz}}{\partial r}+\frac{1}{r}\frac{\partial\sigma_{\theta z}}{\partial\theta}+\frac{\partial\sigma_{zz}}{\partial z}+\frac{\sigma_{rz}}{r}= \quad (1)$$

$$\frac{\partial\sigma_{r\theta}}{\partial r}+\frac{1}{r}\frac{\partial\sigma_{\theta\theta}}{\partial\theta}+\frac{\partial\sigma_{\theta z}}{\partial z}+\frac{2\sigma_{r\theta}}{r}=0.$$

– stress tensor $\hat{\sigma}(r,\theta,z)$ satisfies the boundary conditions:

$$\vec{\sigma}_n\equiv(\vec{n}\cdot\hat{\sigma})|_{\partial X}=\vec{\sigma}_n^{+}, \quad (2)$$

where $\vec{\sigma}_n(r,\theta,z)$ – the stress vector on the surface ∂X; $\vec{\sigma}_n^{+}(r,\theta,z)$ – a given vector of surface forces on ∂X; $\vec{n}\equiv n_r\vec{e}_z+n_\theta\vec{e}_\theta+n_z\vec{e}_z=\vec{\nabla}f(r,\theta,z)/\left|\vec{\nabla}f(r,\theta,z)\right|$ – external normal to the body surface ∂X.

In a cylindrical coordinate system, the components of the stress tensor $\hat{\sigma}$ are fed through the deformation tensor $\hat{\varepsilon}$ by the following relationship:

$$\sigma_{rr}=\lambda\vartheta+2\mu\varepsilon_{rr},\quad \sigma_{\theta\theta}=\lambda\vartheta+2\mu\varepsilon_{\theta\theta},\quad \sigma_{zz}=\lambda\vartheta+2\mu\varepsilon_{zz},$$

$$\sigma_{rz}=\mu\varepsilon_{rz},\quad \sigma_{r\theta}=\mu\varepsilon_{r\theta},\quad \sigma_{\theta z}=\mu\varepsilon_{\theta z}, \quad (3)$$

where $\varepsilon_{rr},\varepsilon_{\theta\theta},\varepsilon_{zz},\varepsilon_{rz},\varepsilon_{r\theta},\varepsilon_{\theta z}$ are the components of the deformation tensor $\hat{\varepsilon}$; μ,λ - elastic Lamé constants.

The deformation tensor $\hat{\varepsilon}$ is expressed in terms of the components of the displacement vector $\vec{u}(u_r,u_\theta,u_z)$ as follows:

$$(4)\quad \varepsilon_{rr}=\frac{\partial U_r}{\partial r},\qquad \varepsilon_{\theta\theta}=\frac{1}{r}\frac{\partial U_\theta}{\partial\theta}+\frac{U_r}{r},\qquad \varepsilon_{zz}=\frac{\partial U_z}{\partial z},$$

$$\varepsilon_{rz}=\frac{\partial U_r}{\partial z}+\frac{\partial U_z}{\partial r},\varepsilon_{r\theta}=\frac{\partial U_\theta}{\partial r}-\frac{U_\theta}{r}+\frac{1}{r}\frac{\partial U_r}{\partial\theta},\varepsilon_{\theta z}=\frac{1}{r}\frac{\partial U_z}{\partial\theta}+\frac{\partial U_\theta}{\partial z}.$$

Volumetric deformation ϑ is calculated by the formula:

$$(5)\qquad \vartheta=\varepsilon_{rr}+\varepsilon_{\theta\theta}+\varepsilon_{zz}=\frac{\partial U_r}{\partial r}+\frac{1}{r}\frac{\partial U_\theta}{\partial\theta}+\frac{U_r}{r}+\frac{\partial U_z}{\partial z}.$$

3.1. Formulation of the boundary value problem of the elasticity theory in Dugall's harmonic potential

Consider the representation of the components of the displacement vector $\vec{u}$ proposed by J.Dugall [11] through three harmonic spatial functions $\varphi(r,\theta,z),\omega(r,\theta,z),\psi(r,\theta,z)$, which was in among the first approaches to construct the solution of equilibrium equations (1) of the linear elasticity theory in displacements in three-dimensional space:

$$(6)\quad \begin{aligned} U_r&=2z\frac{\partial^2\varphi}{\partial r\partial z}+(3-4v)\frac{\partial\varphi}{\partial r}+\frac{\partial\omega}{\partial r}+\frac{2}{r}\frac{\partial\psi}{\partial\theta},\\ U_\theta&=\frac{2z}{r}\frac{\partial^2\varphi}{\partial\theta\partial z}+\frac{3-4v}{r}\frac{\partial\varphi}{\partial\theta}+\frac{1}{r}\frac{\partial\omega}{\partial\theta}-2\frac{\partial\psi}{\partial r},\\ U_z&=2z\frac{\partial^2\varphi}{\partial z^2}-(3-4v)\frac{\partial\varphi}{\partial z}+\frac{\partial\omega}{\partial z}. \end{aligned}$$

where v - the Poisson's ratio.

Substituting the components of the displacement vector (6) in the ratio of the deformation tensor (4), we obtain:

$$\begin{aligned} \varepsilon_{rr}&=2z\frac{\partial^3\varphi}{\partial r^2\partial z}+(3-4v)\frac{\partial^2\varphi}{\partial r^2}+\frac{\partial^2\omega}{\partial r^2}+\frac{2}{r}\frac{\partial^2\psi}{\partial r\partial\theta}-\frac{2}{r^2}\frac{\partial\psi}{\partial\theta},\\ \varepsilon_{\theta\theta}&=\frac{2z}{r^2}\frac{\partial^3\varphi}{\partial\theta^2\partial z}+\frac{3-4v}{r^2}\frac{\partial^2\varphi}{\partial\theta^2}+\frac{2z}{r}\frac{\partial^2\varphi}{\partial r\partial z}+\frac{(3-4v)}{r}\frac{\partial\varphi}{\partial r}+\\ &+\frac{1}{r^2}\frac{\partial^2\omega}{\partial\theta^2}+\frac{1}{r}\frac{\partial\omega}{\partial r}-\frac{2}{r}\frac{\partial^2\psi}{\partial\theta\partial r}+\frac{2}{r^2}\frac{\partial\psi}{\partial\theta},\\ \varepsilon_{zz}&=2z\frac{\partial^3\varphi}{\partial z^3}-(1-4v)\frac{\partial^2\varphi}{\partial z^2}+\frac{\partial^2\omega}{\partial z^2},\\ \varepsilon_{rz}&=2\left(2z\frac{\partial^3\varphi}{\partial r\partial z^2}+\frac{\partial^2\varphi}{\partial r\partial z}+\frac{\partial^2\omega}{\partial r\partial z}+\frac{1}{r}\frac{\partial^2\psi}{\partial\theta\partial z}\right),\\ \varepsilon_{r\theta}&=2\left(\frac{2z}{r}\frac{\partial^3\varphi}{\partial r\partial\theta\partial z}+\frac{3-4v}{r}\frac{\partial^2\varphi}{\partial r\partial\theta}-\frac{2z}{r^2}\frac{\partial^2\varphi}{\partial\theta\partial z}-\frac{3-4v}{r^2}\frac{\partial\varphi}{\partial\theta}+\right.\\ &\left.+\frac{1}{r}\frac{\partial^2\omega}{\partial r\partial\theta}-\frac{1}{r^2}\frac{\partial\omega}{\partial\theta}-2\frac{\partial^2\psi}{\partial r^2}+\frac{\partial^2\psi}{\partial z^2}\right),\\ \varepsilon_{\theta z}&=2\left(\frac{2z}{r}\frac{\partial^3\varphi}{\partial\theta\partial z^2}+\frac{1}{r}\frac{\partial^2\varphi}{\partial\theta\partial z}+\frac{1}{r}\frac{\partial^2\omega}{\partial\theta\partial z}-\frac{\partial^2\psi}{\partial r\partial z}\right). \end{aligned}\quad (7)$$

Accordingly, the volume deformation ϑ under the conditions of harmony of the functions $\varphi(r,\theta,z)$, $\omega(r,\theta,z)$, $\psi(r,\theta,z)$ is calculated as follows:

$$(8)\qquad \vartheta=\varepsilon_{rr}+\varepsilon_{\theta\theta}+\varepsilon_{zz}=-4(1-2v)\frac{\partial^2\varphi}{\partial z^2}.$$

Based on relations (7) and (8) we find the form of the components of the stress tensor (3):

$$\begin{aligned} \sigma_{rr}&=2\mu\left(2z\frac{\partial^3\varphi}{\partial r^2\partial z}+(3-4v)\frac{\partial^2\varphi}{\partial r^2}-4v\frac{\partial^2\varphi}{\partial z^2}+\frac{\partial^2\omega}{\partial r^2}+\right.\\ &\left.+\frac{2}{r}\frac{\partial^2\psi}{\partial r\partial\theta}-\frac{2}{r^2}\frac{\partial\psi}{\partial\theta}\right),\\ \sigma_{\theta\theta}&=2\mu\left(\frac{2z}{r^2}\frac{\partial^3\varphi}{\partial\theta^2\partial z}+\frac{3-4v}{r^2}\frac{\partial^2\varphi}{\partial\theta^2}-4v\frac{\partial^2\varphi}{\partial z^2}+\frac{2z}{r}\frac{\partial^2\varphi}{\partial r\partial z}+\right.\\ &\left.+\frac{(3-4v)}{r}\frac{\partial\varphi}{\partial r}+\frac{1}{r^2}\frac{\partial^2\omega}{\partial\theta^2}+\frac{1}{r}\frac{\partial\omega}{\partial r}-\frac{2}{r}\frac{\partial^2\psi}{\partial\theta\partial r}+\frac{2}{r^2}\frac{\partial\psi}{\partial\theta}\right),\\ \sigma_{zz}&=2\mu\left(2z\frac{\partial^3\varphi}{\partial z^3}-\frac{\partial^2\varphi}{\partial z^2}+\frac{\partial^2\omega}{\partial z^2}\right),\\ \sigma_{rz}&=2\mu\left(2z\frac{\partial^3\varphi}{\partial r\partial z^2}+\frac{\partial^2\varphi}{\partial r\partial z}+\frac{\partial^2\omega}{\partial r\partial z}+\frac{1}{r}\frac{\partial^2\psi}{\partial\theta\partial z}\right),\\ \sigma_{r\theta}&=2\mu\left(\frac{2z}{r}\frac{\partial^3\varphi}{\partial r\partial\theta\partial z}+\frac{3-4v}{r}\frac{\partial^2\varphi}{\partial r\partial\theta}-\frac{2z}{r^2}\frac{\partial^2\varphi}{\partial\theta\partial z}-\right.\\ &\left.-\frac{3-4v}{r^2}\frac{\partial\varphi}{\partial\theta}+\frac{1}{r}\frac{\partial^2\omega}{\partial r\partial\theta}-\frac{1}{r^2}\frac{\partial\omega}{\partial\theta}-2\frac{\partial^2\psi}{\partial r^2}-\frac{\partial^2\psi}{\partial z^2}\right),\\ \sigma_{\theta z}&=2\mu\left(\frac{2z}{r}\frac{\partial^3\varphi}{\partial\theta\partial z^2}+\frac{1}{r}\frac{\partial^2\varphi}{\partial\theta\partial z}+\frac{1}{r}\frac{\partial^2\omega}{\partial\theta\partial z}-\frac{\partial^2\psi}{\partial r\partial z}\right). \end{aligned}\quad (9)$$

Based on the normal components of the stress tensor $\sigma_{rr},\sigma_{\theta\theta},\sigma_{zz}$ we find its first invariant:

$$(10)\qquad J=\sigma_{rr}+\sigma_{\theta\theta}+\sigma_{zz}=-8\mu(v+1)\frac{\partial^2\varphi}{\partial z^2}.$$

Thus, using the representation of the fundamental solution of equilibrium equations in the Dugall's form, the boundary value problem of the linear theory of elasticity (1) - (2) is reformulated into a boundary value problem for harmonic scalar potentials:

$$(11)\qquad \Delta\big(\varphi(r,\theta,z),\omega(r,\theta,z),\psi(r,\theta,z)\big)=0,$$

which satisfy the corresponding boundary conditions on the surface ∂X:

$$\begin{aligned} (\vec{n}\cdot\hat{\sigma})|_{\partial X}&=\big((n_r\sigma_{rr}+n_\theta\sigma_{r\theta}+n_z\sigma_{rz})\overrightarrow{e_r}+\\ &+(n_r\sigma_{r\theta}+n_\theta\sigma_{\theta\theta}+n_z\sigma_{\theta z})\overrightarrow{e_\theta}+\\ &+(n_r\sigma_{rz}+n_\theta\sigma_{\theta z}+n_z\sigma_{zz})\overrightarrow{e_z}\big)|_{\partial X}=\vec{\sigma}_n^+, \end{aligned}\quad (12)$$

where $\Delta\equiv\vec{\nabla}\cdot\vec{\nabla}=\frac{\partial^2}{\partial r^2}+\frac{1}{r}\frac{\partial}{\partial r}+\frac{1}{r^2}\frac{\partial^2}{\partial\theta^2}+\frac{\partial^2}{\partial z^2}$ – Laplace operator. $\vec{\nabla}=\frac{\partial}{\partial r}\overrightarrow{e_r}+\frac{1}{r}\frac{\partial}{\partial\theta}\overrightarrow{e_\theta}+\frac{\partial}{\partial z}\overrightarrow{e_z}$ – Hamilton operator.

3.2. Statement of axisymmetric problems of the elasticity theory in harmonic potentials

Let the axis of symmetry of the body coincide with the axis z of the cylindrical coordinate system (r,θ,z). Given that the problem is axisymmetric, the displacement vector $\vec{u}$ does not depend on the angle θ:

$$(13)\qquad \frac{\partial\vec{u}}{\partial\theta}=0.$$

Given this ratio, the following conditions are imposed on the components of the displacement vector $\vec{u}$ in the Dugall's form (6):

$$\begin{aligned} \frac{\partial U_r}{\partial\theta}&=2z\frac{\partial^3\varphi}{\partial r\partial\theta\partial z}+(3-4v)\frac{\partial^2\varphi}{\partial r\partial\theta}+\frac{\partial^2\omega}{\partial r\partial\theta}+\frac{2}{r}\frac{\partial^2\psi}{\partial\theta^2}=0,\\ \frac{\partial U_\theta}{\partial\theta}&=\frac{2z}{r}\frac{\partial^3\varphi}{\partial\theta^2\partial z}+\frac{3-4v}{r}\frac{\partial^2\varphi}{\partial\theta^2}+\frac{1}{r}\frac{\partial^2\omega}{\partial\theta^2}-2\frac{\partial^2\psi}{\partial r\partial\theta}=0,\\ \frac{\partial U_z}{\partial\theta}&=2z\frac{\partial^3\varphi}{\partial\theta\partial z^2}-(3-4v)\frac{\partial^2\varphi}{\partial\theta\partial z}+\frac{\partial^2\omega}{\partial\theta\partial z}=0. \end{aligned}\quad (14)$$

From these conditions it follows that the harmonic functions $\varphi(r,\theta,z)$, $\omega(r,\theta,z)$ and $\psi(r,\theta,z)$ are linear functions on the variable θ, and we also get some elms on these functions, in particular:

$$\frac{\partial^2\omega}{\partial r\partial\theta}=-2z\frac{\partial^3\varphi}{\partial r\partial\theta\partial z}-(3-4v)\frac{\partial^2\varphi}{\partial r\partial\theta},$$

$$\frac{\partial^2\psi}{\partial r\partial\theta}=0, \tag{15}$$

$$\frac{\partial^2\omega}{\partial\theta\partial z}=-2z\frac{\partial^3\varphi}{\partial\theta\partial z^2}+(3-4v)\frac{\partial^2\varphi}{\partial\theta\partial z}.$$

Accordingly, the components of the deformation tensor $\hat{\varepsilon}$ (7) take the form:

$$\varepsilon_{rr}=2z\frac{\partial^3\varphi}{\partial r^2\partial z}+(3-4v)\frac{\partial^2\varphi}{\partial r^2}+\frac{\partial^2\omega}{\partial r^2}-\frac{2}{r^2}\frac{\partial\psi}{\partial\theta},$$

$$\varepsilon_{\theta\theta}=\frac{2z}{r}\frac{\partial^2\varphi}{\partial r\partial z}+\frac{3-4v}{r}\frac{\partial\varphi}{\partial r}+\frac{1}{r}\frac{\partial\omega}{\partial r}+\frac{2}{r^2}\frac{\partial\psi}{\partial\theta},$$

$$\varepsilon_{zz}=2z\frac{\partial^3\varphi}{\partial z^3}-(1-4v)\frac{\partial^2\varphi}{\partial z^2}+\frac{\partial^2\omega}{\partial z^2},$$

$$\varepsilon_{rz}=2\left(2z\frac{\partial^3\varphi}{\partial r\partial z^2}+\frac{\partial^2\varphi}{\partial r\partial z}+\frac{\partial^2\omega}{\partial r\partial z}+\frac{1}{r}\frac{\partial^2\psi}{\partial\theta\partial z}\right),$$

$$\varepsilon_{r\theta}=2\left(-\frac{2z}{r^2}\frac{\partial^2\varphi}{\partial\theta\partial z}-\frac{3-4v}{r^2}\frac{\partial\varphi}{\partial\theta}-\frac{1}{r^2}\frac{\partial\omega}{\partial\theta}-\frac{\partial^2\psi}{\partial r^2}+\frac{1}{r}\frac{\partial\psi}{\partial r}\right),$$

$$\varepsilon_{\theta z}=2\left(\frac{4(1-v)}{r}\frac{\partial^2\varphi}{\partial\theta\partial z}-\frac{\partial^2\psi}{\partial r\partial z}\right). \tag{16}$$

The components of the stress tensor $\hat{\sigma}$, according to (16), are as follows:

$$\sigma_{rr}=2\mu\left(2z\frac{\partial^3\varphi}{\partial r^2\partial z}+(3-4v)\frac{\partial^2\varphi}{\partial r^2}-4v\frac{\partial^2\varphi}{\partial z^2}+\frac{\partial^2\omega}{\partial r^2}-\frac{2}{r^2}\frac{\partial\psi}{\partial\theta}\right),$$

$$\sigma_{\theta\theta}=2\mu\left(\frac{2z}{r}\frac{\partial^2\varphi}{\partial r\partial z}-4v\frac{\partial^2\varphi}{\partial z^2}+\frac{3-4v}{r}\frac{\partial\varphi}{\partial r}+\frac{1}{r}\frac{\partial\omega}{\partial r}+\frac{2}{r^2}\frac{\partial\psi}{\partial\theta}\right),$$

$$\sigma_{zz}=2\mu\left(2z\frac{\partial^3\varphi}{\partial z^3}-\frac{\partial^2\varphi}{\partial z^2}+\frac{\partial^2\omega}{\partial z^2}\right),$$

$$\sigma_{rz}=2\mu\left(2z\frac{\partial^3\varphi}{\partial r\partial z^2}+\frac{\partial^2\varphi}{\partial r\partial z}+\frac{\partial^2\omega}{\partial r\partial z}+\frac{1}{r}\frac{\partial^2\psi}{\partial\theta\partial z}\right),$$

$$\sigma_{r\theta}=2\mu\left(-\frac{2z}{r^2}\frac{\partial^2\varphi}{\partial\theta\partial z}-\frac{3-4v}{r^2}\frac{\partial\varphi}{\partial\theta}-\frac{1}{r^2}\frac{\partial\omega}{\partial\theta}-\frac{\partial^2\psi}{\partial r^2}+\frac{1}{r}\frac{\partial\psi}{\partial r}\right),$$

$$\sigma_{\theta z}=2\mu\left(\frac{4(1-v)}{r}\frac{\partial^2\varphi}{\partial\theta\partial z}-\frac{\partial^2\psi}{\partial r\partial z}\right). \tag{17}$$

Based on the elms (15), the first invariant of the stress tensor is expressed only through one harmonic scalar function $\varphi(r,\theta,z)$:

$$J=\sigma_{rr}+\sigma_{\theta\theta}+\sigma_{zz}=-8\mu(v+1)\frac{\partial^2\varphi}{\partial z^2}. \tag{18}$$

Therefore, the axisymmetric boundary value problem on the harmonic potentials $\varphi(r,\theta,z)$, $\omega(r,\theta,z)$ and $\psi(r,\theta,z)$ has the form:

$$\Delta\big(\varphi(r,\theta,z),\omega(r,\theta,z),\psi(r,\theta,z)\big)=0, \tag{19}$$

which satisfy the corresponding boundary conditions on the body surface ∂X:

$$\begin{aligned}(\vec{n}\cdot\hat{\sigma})|_{\partial X}=&\big((n_r\sigma_{rr}+n_\theta\sigma_{r\theta}+n_z\sigma_{rz})\overrightarrow{e_r}+\\&+(n_r\sigma_{r\theta}+n_\theta\sigma_{\theta\theta}+n_z\sigma_{\theta z})\overrightarrow{e_\theta}+\\&+(n_r\sigma_{rz}+n_\theta\sigma_{\theta z}+n_z\sigma_{zz})\overrightarrow{e_z}\big)|_{\partial X}=\vec{\sigma}_n^{+},\end{aligned} \tag{20}$$

where the components of the stress tensor $\sigma_{rr},\sigma_{\theta\theta},\sigma_{zz},\sigma_{r\theta},\sigma_{rz},\sigma_{\theta z}$ are given by the relations (17).

3.3. Statement of the boundary value problem of pure torsion

Consider one of the axisymmetric stress states of the body of rotation - pure torsion, which is described when the conditions $U_r=U_z=0$:

$$U_r=2z\frac{\partial^2\varphi}{\partial r\partial z}+(3-4v)\frac{\partial\varphi}{\partial r}+\frac{\partial\omega}{\partial r}+\frac{2}{r}\frac{\partial\psi}{\partial\theta}=0,$$

$$U_\theta=\frac{2z}{r}\frac{\partial^2\varphi}{\partial\theta\partial z}+\frac{3-4v}{r}\frac{\partial\varphi}{\partial\theta}+\frac{1}{r}\frac{\partial\omega}{\partial\theta}-2\frac{\partial\psi}{\partial r},$$

$$U_z=2z\frac{\partial^2\varphi}{\partial z^2}-(3-4v)\frac{\partial\varphi}{\partial z}+\frac{\partial\omega}{\partial z}=0. \tag{20}$$

Given the relation (20), the components of the deformation tensor $\hat{\varepsilon}$ (16) and, accordingly, its first invariant ϑ take the form:

$$\varepsilon_{rr}=2z\frac{\partial^3\varphi}{\partial r^2\partial z}+(3-4v)\frac{\partial^2\varphi}{\partial r^2}+\frac{\partial^2\omega}{\partial r^2}-\frac{2}{r^2}\frac{\partial\psi}{\partial\theta}=0,$$

$$\varepsilon_{\theta\theta}=\frac{2z}{r}\frac{\partial^2\varphi}{\partial r\partial z}+\frac{3-4v}{r}\frac{\partial\varphi}{\partial r}+\frac{1}{r}\frac{\partial\omega}{\partial r}+\frac{2}{r^2}\frac{\partial\psi}{\partial\theta}=0,$$

$$\varepsilon_{zz}=2z\frac{\partial^3\varphi}{\partial z^3}-(1-4v)\frac{\partial^2\varphi}{\partial z^2}+\frac{\partial^2\omega}{\partial z^2}=0,$$

$$\varepsilon_{rz}=2\left(2z\frac{\partial^3\varphi}{\partial r\partial z^2}+\frac{\partial^2\varphi}{\partial r\partial z}+\frac{\partial^2\omega}{\partial r\partial z}+\frac{1}{r}\frac{\partial^2\psi}{\partial\theta\partial z}\right)=0,$$

$$\varepsilon_{r\theta}=2\left(-\frac{2z}{r^2}\frac{\partial^2\varphi}{\partial\theta\partial z}-\frac{3-4v}{r^2}\frac{\partial\varphi}{\partial\theta}-\frac{1}{r^2}\frac{\partial\omega}{\partial\theta}-\frac{\partial^2\psi}{\partial r^2}+\frac{1}{r}\frac{\partial\psi}{\partial r}\right)$$

$$\varepsilon_{\theta z}=2\left(\frac{4(1-v)}{r}\frac{\partial^2\varphi}{\partial\theta\partial z}-\frac{\partial^2\psi}{\partial r\partial z}\right). \tag{21}$$

$$\vartheta=\varepsilon_{rr}+\varepsilon_{\theta\theta}+\varepsilon_{zz}=-4(1-2v)\frac{\partial^2\varphi}{\partial z^2}=0. \tag{22}$$

Based on relations (21)-(22), the components of the stress tensor $\hat{\sigma}$ are written as follows:

$$\sigma_{rr}=0,\quad \sigma_{\theta\theta}=0,\quad \sigma_{zz}=0,\quad \sigma_{rz}=0,$$

$$\sigma_{r\theta}=2\mu\left(-\frac{2z}{r^2}\frac{\partial^2\varphi}{\partial\theta\partial z}-\frac{3-4v}{r^2}\frac{\partial\varphi}{\partial\theta}-\frac{1}{r^2}\frac{\partial\omega}{\partial\theta}-\frac{\partial^2\psi}{\partial r^2}+\frac{1}{r}\frac{\partial\psi}{\partial r}\right),$$

$$\sigma_{\theta z}=2\mu\left(\frac{4(1-v)}{r}\frac{\partial^2\varphi}{\partial\theta\partial z}-\frac{\partial^2\psi}{\partial r\partial z}\right). \tag{23}$$

and, accordingly, the first invariant J is identically equal to zero.

Under the axisymmetric problem (15) and the torsion problem (21) - (22) we write the relation:

$$\frac{\partial^2\psi}{\partial r\partial\theta}=0,\qquad \frac{\partial^2\varphi}{\partial z^2}=0,$$

$$2z\frac{\partial^3\varphi}{\partial z^3}-(1-4v)\frac{\partial^2\varphi}{\partial z^2}+\frac{\partial^2\omega}{\partial z^2}=0. \tag{24}$$

on the basis of which we obtain the equations for harmonic functions:

$$\frac{\partial^2\psi}{\partial r\partial\theta}=0,\quad \frac{\partial^2\omega}{\partial z^2}=0,\quad \frac{\partial^2\varphi}{\partial z^2}=0. \tag{25}$$

Under these conditions, we present the structure of harmonic potentials $\varphi(r,\theta,z)$, $\omega(r,\theta,z)$ and $\psi(r,\theta,z)$ in the form:

$$\begin{aligned}\psi(r,\theta,z)&=\psi_0(r,z)+\psi_1(\theta,z)+\psi_2(z),\\ \varphi(r,\theta,z)&=\varphi_0(r,\theta)+z\varphi_1(r,\theta),\\ \omega(r,\theta,z)&=\omega_0(r,\theta)+z\omega_1(r,\theta).\end{aligned} \tag{26}$$

where $\psi_i, \varphi_j, \omega_j, (i=\overline{0,2})(j=\overline{0,1})$ – unknown harmonic functions.

Note that $\psi_1(\theta,z)$ and $\psi_2(z)$ do not affect the structure of the tangential components of the stress tensor $\sigma_{r\theta}$ and $\sigma_{\theta z}$, so they can be considered equal to zero.

4. Results and discussion

The obtained structure of harmonic functions (26) is substituted into the initial representation of the displacement vector $\vec{u}$ (20) for the pure torsion problem. We obtain finite expressions and connections for unknown harmonic functions $\psi_0(r,z)$, $\varphi_0(r,\theta)$, $\varphi_1(r,\theta)$, $\omega_0(r,\theta)$, $\omega_1(r,\theta)$:

$$U_r = \frac{\partial}{\partial r}\left((3-4v)\varphi_0 + 8(1-v)z\varphi_1 + \omega_0\right) = 0,$$

$$U_\theta = \frac{\partial}{\partial \theta}\left[\frac{1}{r}\left((3-4v)\varphi_0 + 8(1-v)z\varphi_1 + \omega_0\right)\right] - 2\frac{\partial \psi_0}{\partial r},$$

$$U_z = -(3-4v)\varphi_1 + \omega_1 = 0. \quad (27)$$

Based on these relations, we present the components of the stress tensor $\hat{\sigma}$ through new harmonic potentials $\varphi_0(r,\theta)$, $\varphi_1(r,\theta)$, $\omega_0(r,\theta)$, $\psi_0(r,z)$:

$$\sigma_{rr} = 0, \quad \sigma_{\theta\theta} = 0, \quad \sigma_{zz} = 0, \quad \sigma_{rz} = 0,$$

$$\sigma_{r\theta} = 2\mu\left(\frac{1}{r^2}\left((4v-3)\frac{\partial \varphi_0(r,\theta)}{\partial \theta} - 8(1-v)z\frac{\partial \varphi_1(r,\theta)}{\partial \theta}\right) - \right.$$

$$\left. -\frac{1}{r^2}\left(\frac{\partial \omega_0(r,\theta)}{\partial \theta}\right) - \left(\frac{\partial^2 \psi_0(r,z)}{\partial r^2} - \frac{1}{r}\frac{\partial \psi_0(r,z)}{\partial r}\right)\right),$$

$$\sigma_{\theta z} = 2\mu\left(\left(\frac{4(1-v)}{r}\frac{\partial \varphi_1(r,\theta)}{\partial \theta}\right) - \left(\frac{\partial^2 \psi_0(r,z)}{\partial r \partial z}\right)\right). \quad (28)$$

Thus, the boundary value problem of pure torsion of the theory of elasticity for canonical bodies is reformulated into a boundary value problem on harmonic potentials $\varphi_0(r,\theta)$, $\varphi_1(r,\theta)$, $\omega_0(r,\theta)$, $\psi_0(r,z)$:

$$\Delta\left(\varphi_0(r,\theta),\ \varphi_1(r,\theta), \omega_0(r,\theta),\ \psi_0(r,z)\right) = 0,$$

which satisfy the corresponding boundary conditions on the body surface ∂X:

$$(\vec{n}\cdot\hat{\sigma})|_{\partial X} = \left((n_\theta\sigma_{r\theta})\overrightarrow{e_r} + (n_r\sigma_{r\theta} + n_z\sigma_{\theta z})\overrightarrow{e_\theta} + (n_\theta\sigma_{\theta z})\overrightarrow{e_z}\right) =$$

$$= 2\mu\left(\left[n_r\left(\frac{1}{r^2}\left((4v-3)\frac{\partial \varphi_0(r,\theta)}{\partial \theta} - 8(1-v)\,z\frac{\partial \varphi_1(r,\theta)}{\partial \theta}\right) - \right.\right.$$

$$\left. -\frac{1}{r^2}\left(\frac{\partial \omega_0(r,\theta)}{\partial \theta}\right) - \left(\frac{\partial^2 \psi_0(r,z)}{\partial r^2} - \frac{1}{r}\frac{\partial \psi_0(r,z)}{\partial r}\right)\right]\overrightarrow{e_r} +$$

$$+\left[n_r\left(\frac{1}{r^2}\left((4v-3)\frac{\partial \varphi_0(r,\theta)}{\partial \theta} - 8(1-v)\,z\frac{\partial \varphi_1(r,\theta)}{\partial \theta}\right) - \right.\right.$$

$$\left. -\frac{1}{r^2}\left(\frac{\partial \omega_0(r,\theta)}{\partial \theta}\right) - \left(\frac{\partial^2 \psi_0(r,z)}{\partial r^2} - \frac{1}{r}\frac{\partial \psi_0(r,z)}{\partial r}\right)\right) +$$

$$\left. +n_z\left(\left(\frac{4(1-v)}{r}\frac{\partial \varphi_1(r,\theta)}{\partial \theta}\right) - \left(\frac{\partial^2 \psi_0(r,z)}{\partial r \partial z}\right)\right)\right]\overrightarrow{e_\theta} +$$

$$\left. +\left[n_\theta\left(\left(\frac{4(1-v)}{r}\frac{\partial \varphi_1(r,\theta)}{\partial \theta}\right) - \left(\frac{\partial^2 \psi_0(r,z)}{\partial r \partial z}\right)\right)\right]\overrightarrow{e_z}\right)\Bigg|_{\partial X} = \vec{\sigma}_n^+.$$

5. Conclusion

Based on the representation of the fundamental solution of the linear elasticity theory of the mechanics of a deformable solid in the form of J.Dougall through the spatial harmonic functions $\varphi(r,\theta,z)$, $\omega(r,\theta,z)$, $\psi(r,\theta,z)$, the axisymmetric problem of the theory of elasticity in a cylindrical coordinate system for bodies bounded by a canonical surface was formulated.

The case of the pure torsion problem is considered and the elastic characteristics are given, namely, the components of deformation tensors $\hat{\varepsilon}$ and stresses $\hat{\sigma}$ and the structure of the corresponding external loads on the side surface of a given isotropic elastic body in the above-mentioned harmonic potentials. The elms on the initial basic harmonic functions in the Dougall's form are obtained, which made it possible to concretize their structure and submit through new harmonic potentials $\varphi_0(r,\theta)$, $\varphi_1(r,\theta)$, $\omega_0(r,\theta)$, $\psi_0(r,z)$ and formulate an appropriate boundary value problem.

6. Literature

1. W.Kelvin, P.g.Tait. Treatise on natural philosophy. – Cambridge: Univ. press, (1879) 328 p.
2. M.J.Boussinesq. Application des potentials a l'etude de lequilibre et du movement des solides elastiques. – Paris: Gauthiers-Vilars, (1885) 280 p.
3. B.Galerkin. K obshemu resheniyu zadach teoriyi uprugosti v trjoch izmereniyach s pomochju funkciy napryazeniy i peremeshcheniy. Doklady AN SSSR,ser A.(10) (1931) 281-286. [InRussian].
4. P.F. Papkovich Teoriya uprugosty, Oborongiz, Moscow, 1939, 639 p. [In Russian] .
5. H. Neuber. Concentratsiya napriazeniy, Gostechizdat, Moscow, 1947, 204 p. [In Russian].
6. Revenko V.P. Solving the three-dimensional equations of the linear theory of elasticity. Int. Appl. Mech. 45 (7), (2009) 730-741.
7. Revenko V.P. Pobudova zahalnoho rozviazku tryvymirnykh rivnian Liame teorii pruzhnosti v kryvoliniinii systemi koordynat. Matematychnyi visnyk Naukovoho tovarystva im.Shevchenka. 2., (2005) 185-198 [InUkrainian].
8. Revenko V.P. Rozviazannia tryvymirnoi kraiovoi zadachi teorii pruzhnosti dlia tila obertannia. Prykladni problemy mekhaniky i matematyky. 12, (2014) 130–136 [InUkrainian].
9. A.I. Lurie Teoriya uprugosty, Nauka, Moscow, 1970, 940 p. [In Russian].
10. S.P.Timoshenko, J.N. Goodier Teoriya uprugosty, Nauka, Moscow, 1975, 575 p. [In Russian].
11. J.Dougall. An analytical theory of the equilibrium of an isotropic elastic plate. Trans. Roy. Soc. Edinburgh. 41(8),(1904) 129-228.
12. Yu.Tokovyi. Funktcii napruzen tryvymirnoi zadachi teorii pruznosti dlya sutsilnogo skinchennogo cylindra. Visnyk KNU, 27 (2012) 50-54. [InUkrainian] (V. Meleshko).

Consistent Presentation of the Beam Deflection Theory Including Shear Correction

Rumen Krastev
Institute of Mechanics - Bulgarian Academy of Sciences
Email: r_krastev@imbm.bas.bg

Abstract: *This article explains a mathematically consistent approach for solving the equations of Timoshenko's beam theory for statically loaded beams. Theoretic sections 3.4 - 3.5 give a good description of the shear deformation and the primary approach for calculating deflections of beams under bending, taking into account both causes for deflection: bending moment and shear force. Values for the shear correction factor are discussed in section 4. This work was started to check the validity of an equation for deflection of a symmetrically loaded short rectangular beam with span/height ratio = 3 under four-point bending with upper-span/span ratio = 1/3. The exact solution is not presented here, but we can confirm that the presented theory, when applied for the mentioned loading scheme, leads to this equation using a shear correction factor k = 5/6.*
Keywords*: EULER-BERNOULLI, TIMOSHENKO BEAM THEORY, DEFLECTION, SHEAR DEFORMATION, SHEAR COEFFICIENT*

1. Introduction

Many structural members in working conditions are subjected to bending. Usually, the bending is not pure, i.e. the structural element endures both bending moment and shearing force. These internal forces cause deformation of the beam, i.e. its shape changes. The deviation of the centre of a cross-section from its original position is called *deflection*. It is known for slender beams that deflection caused by the shearing force is negligible.

A practical problem for determining the exact deflection of short rectangular beams under four-point bending raises the need to clarify the theory, more precisely, the theoretical base of the following equation, published in standard ASTM C1018-97.

$$f = \frac{23F}{1296EI} l^3 \left(1 + \frac{216(1+\nu)}{115}\left(\frac{h}{l}\right)^2\right) \tag{1}$$

Where f is the deflection of the neutral plane, F is the load, l is the span, E is the estimated elastic modulus, I is the second moment of area, h is the specimen height, and ν is the Poisson's ratio. The mentioned standard is related to the test method ASTM C78 that requires the span length to be three times the specimen depth (l/h = 3) and *upper-span/span* = 1/3.

2. Synopsis of the historical development

An approach is known for calculating the deflection caused by bending moment with main contributors of Jacob Bernoulli, Daniel Bernoulli and Leonard Euler, [1]. When considering deflection of a cantilever beam, loaded at the free end by force F, Euler [1, p. 45] reached the differential equation (2):

$$C\frac{w''}{(1+w'^2)^{3/2}} = Fx \tag{2}$$

Where x is the distance from the point of application of the force to a cross-section under consideration, C is constant, w is the deflection of the centre of the cross-section, $w' = \frac{dw}{dx}$ and $w'' = \frac{d^2w}{dx^2}$.

In the real constructions, small deflections are considered usually. In this case, the rotation angle is minimal, respectively $w' \ll 1$, and for engineering purposes, the simplified equation (3) is solved:

$$Cw'' = Fx \tag{3}$$

Later, Saint Venant carefully considered the hypotheses: 1. the cross-sections in the deformation remain flat, and 2. the adjacent longitudinal fibres do not influence each other, being in a state of tensile or compression [1, p. 164]. He shows that the initially plane cross-sections change their shape due to the tangential stresses acting in the cross-section [1, p. 165]. Saint-Venant has formulated a solution for bending a cylindrical cantilever beam of a constant cross-section by a terminal load [2, p. 316; p. 133].

D. Zhouravski had investigated how shearing stress is distributed by the height of the cross-section and derived a formula for its approximate assessment, see eq. 64 in [3, p. 111-113].

An elementary derivation of the effect of the shearing force on the curvature of the beam has been made by Grashof (1878) and W.J.M Rankine (1895), [2, p. 31].

J.W. Raleigh investigated vibrations of strings, rods, membranes, plates and shells. The author demonstrates some properties that an engineer can extract from the application of *generalised forces* and *generalised coordinates*. The idea of calculating frequencies directly from the energy condition without solving differential equations was subsequently developed by Walter Ritz. The *Rayleigh-Ritz method* is now widely used not only in the study of oscillations but also in solving problems of the theory of elasticity, theory of structures, not linear mechanics and other branches of physics, [1, p. 404].

In the early 20th century, S.P. Timoshenko proposed an approach as an adjunct to the Euler-Bernoulli theory in order to take into account the effect of the transverse force on the transverse vibrations of a cantilever beam [4]. According to it:

$$\frac{dw}{dx} = \varphi + \gamma \tag{4}$$

$$M = -EI\frac{d\varphi}{dx} \tag{5}$$

$$Q = kGA\gamma \tag{6}$$

Where φ is the angle of rotation of the cross-section due to the bending moment M, γ is the angle induced by the tangential force Q, EI is the flexural rigidity of the cross-section, A is the cross-section area, G is the shearing modulus of elasticity and k is "a constant which depend on the cross-section", [4]. This coefficient is introduced because the tangential stress is not distributed evenly along with the height of the cross-section. As it is well known, the tangential stress is zeroth at the upper and lower edge of the cross-section, and it is greatest near the neutral plane. The angle γ can be eliminated from Eqs. (4) and (6):

$$Q = kGA\left(-\varphi + \frac{dw}{dx}\right) \tag{7}$$

In his work [4], Timoshenko analyses the system of equations (5) and (7) in order to determine the effect of tangential force on the frequency of transverse vibrations of a rectangular beam.

In the textbook [3], Timoshenko presents eq. (6) otherwise:

$$\frac{dy_1}{dx} = \frac{cQ}{GA} \tag{8}$$

Where y_1 is *deflection due to shear* and respectively $\gamma = dy_1/dx$. The coefficient c is explained as "a numerical factor with which the average shearing stress (Q/A) must be multiplied in order to obtain the shearing stress at the centroid of the cross-section", [3, p. 170]. This definition "has been clearly shown to give unsatisfactory results" [5], but the main equations (3)-(7) are still applicable.

Many articles are aiming more precise definition for the shear coefficient and its determination. Based on the Jouravski's formula, one technique is published in the textbook [6] and is presented below in this article.

From the comparison of Eqs. (6) and (8) it can be seen that

(9) $$k = \frac{1}{c} = \frac{Q}{GA\gamma}$$

It should be noted that the term "shear correction factor" is not clearly defined. In most articles, [5, 10, 15 etc.], we could see that it refers to coefficient *k* and eq. (6), but in other works, [6, 11], it refers to the factor *c* and eq. (8). One should use some published shear coefficient with a clear idea for its proper place in the equation.

Most of the textbooks explain well how to calculate the deflection caused by the bending moment - "Euler-Bernoulli Method". However, the deflection caused by the tangential force is not commented or is indicated that it is negligible for long (slender) beams. For example, standard EN ISO 178, [7] requires the use of long specimens, with a *span/height* ratio = 16 for usual specimens. However, for tick fibre-reinforced specimens this ratio should be = 60; for thin specimens – it should be = 8, and for flexible materials it should be = 32.

When we need to work with short beams, the question about the magnitude of the tangential deflection cannot be neglected! Textbooks like [8] and [19] do not explain the Timoshenko beam theory.

There is a significant interest about vibrations of Timoshenko beams in several conditions, [10-15] etc. However, the mathematical apparatus in these publications is too complicated and it is not suitable for easy understanding and assessment of shear deflection of statically loaded beams.

Recently, Ke Gong [20], Ghugal et al. [21] suggested new theories about the deflection of thick beams.

With the purpose of clarifying and gathering on one place these accomplishments, there is a consistent presentation below of the static beam deflection theory, including shear correction.

3. Theoretical approach

3.1 Scheme and coordinate system

Consider a horizontal beam, somehow fixed in space and loaded with forces and distributed loads. We use a coordinate system with the *x*-axis to the right, *y* to us and *z* – downward (Fig. 1). We consider a situation in which the loads are directed in the vertical direction *z*.

3.2 Load and support reactions

The equilibrium conditions of the beam are considered. From these equations are find the support reactions, i.e. forces and moments at the anchorage points, depending on the loads applied to the beam.

3.3 Internal forces in the beam

The beam is divided into segments, with borders - where there is a concentrated load or at the ends of the distributed loads. These segments are examined sequentially. For each segment, a mental cut is made through the beam at a distance *x* from the end of the beam. Fig. 1 illustrate a beam segment under distributed load, mentally cut at distance *x*.

By applying the equilibrium conditions, we find the dependences of the tangential force Q_z on x and the bending moment M_y on *x*. The following dependencies apply in all cases:

(9) $$\frac{dQ_z}{dx} = -q(x)$$

(10) $$\frac{dM_y}{dx} = Q_z(x)$$

Here, q is the load distributed on the beam. For example, the load by the weight of the beam.

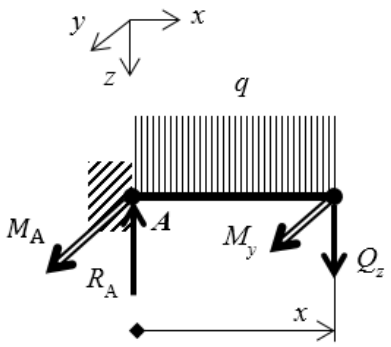


Fig. 1 *beam section under distributed load, fixed in point A and mentally cut at distance x.*

Equation (9) shows that the distributed load (in the *z*-direction) causes a tangential force in the beam. Concentrated forces cause the tangential force to jump in the applied points, so these points should be the boundaries of the segments considered.

The tangential force causes a bending moment in the beam, according to Eq. (10).

3.4 Deformation of the beam

The centre line of the beam in question coincides with the *x*-axis initially. The deformed state of the beam is described by the equation of the elastic line $w(x)$, which indicates the deflection, i.e. displacement of the centres of the cross-sections in the *z*-direction.

It is known that bending moment causes bending (flexure) of the beam, which changes its shape. This is expressed by a change in the slope and position of the cross-sections under consideration in the plane *xz*, Eq. (5).

It is known that tangential force causes a tangential displacement between adjacent cross-sections of the beam, increasing the rotation of the cross-sections by an angle γ, Eq. (6).

Timoshenko considers the bending as a sum of two components, Eq. (4). In integral form, the overall deflection also has two parts: deflection due to bending moment and deflection due to shear force.

(11) $$w = w_M + w_Q$$

Bernoulli-Euler's theory only considers deflection caused by the bending moment, and the second component is neglected. This is acceptable for slender beams.

3.4.1 Deflection due to bending moment

The bending moment M_y causes an elastic bending and rotation of the beam, which, for small deflections, is described by the equation:

(12) $$EI\frac{d\alpha}{dx} = M_y(x)$$

Where: $d\alpha$ is the angle between two initially collinear cross-sections, on a distance dx from each other, E – elastic modulus of the material, I – area moment of the cross-section. The solution of the differential equation (12) gives the angle of rotation α of the cross-section under consideration, generated by the bending moment, depending on the position *x* of the section.

Deflection of a section under consideration depends on its slope: $dw_M/dx = -\mathrm{tg}(\alpha)$. At small angles $\alpha \cong \mathrm{tg}(\alpha)$ and deflection due to bending moment can be sought according to equation (13):

(13) $$\frac{dw_M}{dx} = -\alpha(x)$$

After the determination of the internal forces, by integrating Eqs. (12) and (13) one can find the deflection caused by the change in beam shape due to the bending moment.

(14) $$w_M(x) = -\int \alpha(x)dx$$

3.4.2 Deflection due to shear force

The tangential force Q_z causes a displacement of adjacent cross-sections in a tangential direction, known as shearing or sliding. It is known that tangential stress has some distribution $\tau_{xz}(y,z)$ over the cross-section – Fig. 2 B). However, if we do not know the exact distribution, or it is too complicated, we could use a simplified - rectangular distribution of the stress (or average shear stress):

(15) $$\tau_R = \frac{Q_z}{A}$$

in combination with some correction factor. Here A is the cross-sectional area. In this case (of rectangular distribution), for the elastic angular deformation of an elementary volume with thickness dx, the Hooke's law is:

(16) $$\frac{Q_z}{A} = -G\gamma = G\frac{dw_Q}{dx}$$

Where G is the shear modulus of elasticity and dw_Q is the tangential displacement between the two sides of this volume. These ideas are visualised in Fig. 2. The angle γ presents the difference between deformed shape by Q (DS Q) and un-deformed shape by Q (UDS Q). The angle γ here is assumed as negative and therefore (-γ) is positive when $Q_z > 0$. This section is in equilibrium because the shearing force generates a bending moment, $dM_y = Q_z dx$, but near cross-sections hold it.

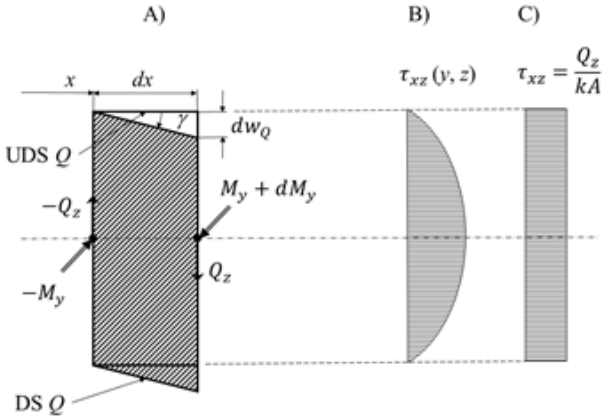


***Fig.2** Simplifying the scheme for shearing. A) Angular deformation of cross-section by transverse shear force. B) Real distribution of the shear stress. C) An assumption for simplified and corrected – rectangular distribution of the shear stress.*

In his paper [4], S.P. Timoshenko does not discuss a hypothetic rectangular distribution that should generate the same deflection as the actual distribution of tangential stresses. However, he introduced a correction factor k (Shear correction factor, Timoshenko shear coefficient) in Eq. (6). It takes into account the fact that used average shear stress (Q_z/A) must be corrected so that it has the same effect as the actual distribution of the stress (as shown in Fig. 2 C).

In the present work, the shear force is considered as known, and the shear displacement is sought:

(17) $$\frac{dw_Q}{dx} = \frac{Q_z(x)}{kGA}$$

Shearing deflection of a beam with variable cross-section is found by solving Eq. (18):

(18) $$w_Q(x) = \int \frac{Q_z(x)}{kGA(x)}dx$$

When considering beams with constant cross-section and using eq. (10), the equation (19) holds:

(19) $$w_Q(x) = \frac{1}{kGA}M_y(x) + C$$

Therefore, the sag pattern is similar to the bending moment diagram for beams with a constant cross-section. The integration constant C is determined according to a known boundary condition.

3.5 Calculation of the shear correction factor

For beams subjected to bending, in the Timoshenko's equation (6), the Q/A ratio represents some mean tangential stress of the section. However, it is known that the actual tangential stress is zero at the upper end and at the lower ends of the section, and it is maximal at the neutral line. To express the dependence of the tangential stresses τ_{xz} on the coordinate (height) z, for a cross-section of arbitrary shape, one usually uses the approximate formula proposed by D. Zhuravskii:

(20) $$\tau_{xz} = \frac{Q_z S_y(z)}{b(z).I_y}$$

Where:

Q_z – Shear force for the cross-section under consideration with coordinate x,

I_y – The second area moment with regard to y-axis.

$b(z)$ – Length of the dense part of the cross-section with coordinate z. For a rectangular section, b is constant.

$S_y(z) = \int_z^{zc} z.dA$ – Static moment of the dense part of the cross-section, bounded by the straight-line $b(z)$ and the outer contour (zc) of the cross-section.

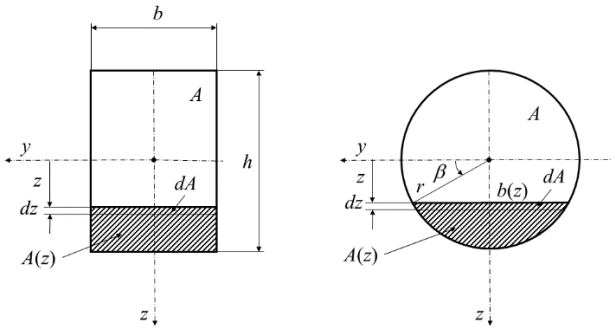


***Fig. 3** Schemes for rectangular cross-section and circular cross-section, explaining the variables in Zhuravskii's formula and Eq. (23), [6, p. 295].*

If we consider a hypothetic situation in which the tangential force is evenly distributed in a cross-section with area A and thickness dx, then the accumulated (specific) potential energy in this section would be:

(21) $$\frac{dU_Q}{dx} = \frac{Q_z^2}{2GA}$$

When considering the same cross-section, but using a distribution of the shear stress according to the Zhuravskii's formula, then this potential energy is given by Eq. (22), [6, p. 294]:

(22) $$\frac{dU_Q}{dx} = \frac{cQ_z^2}{2GA}$$

Formula (23) is obtained for the correction coefficient c.

(23) $$c = \frac{A}{I_y^2}\int_A \frac{S_y^2(z)}{b^2(z)}dA$$

As it was stated above, the static moment is calculated for the dense part of the cross-section bounded between line $b(z)$ and the outer contour.

The correction coefficient *c*, obtained by Eq. (23), could be used in Eq. (8) and other related equations. If one prefers to use the original definition of the Timoshenko's correction factor, Eq. (9) will help.

3.5.1 Correction coefficient for rectangular cross-section

We consider a rectangular section of width b and height h, [6, p. 295] and apply Eq. (23):

$$A = bh, I_y = \frac{bh^3}{12}, b(z) = const.$$

$$S_y(z) = b\left(\frac{h}{2} - z\right).\left(\frac{h}{2} + z\right)/2, dA = bdz$$

(24) $$c_{\blacksquare} = \frac{144.bh}{b^2h^6} 2\int_0^{h/2} \frac{b^2}{4b^2}\left(\frac{h^2}{4} - z^2\right)^2 bdz = \frac{6}{5} = \frac{1}{k_{\blacksquare}}$$

3.5.2 Correction coefficient for circular cross-section

We consider a circular cross-section of radius *r*, [6, p. 295] and find the shear correction factor by Eq. (23):

$$A = \pi r^2, I_y = \pi r^4/4, z = r\sin\beta, b(z) = 2rcos\beta,$$

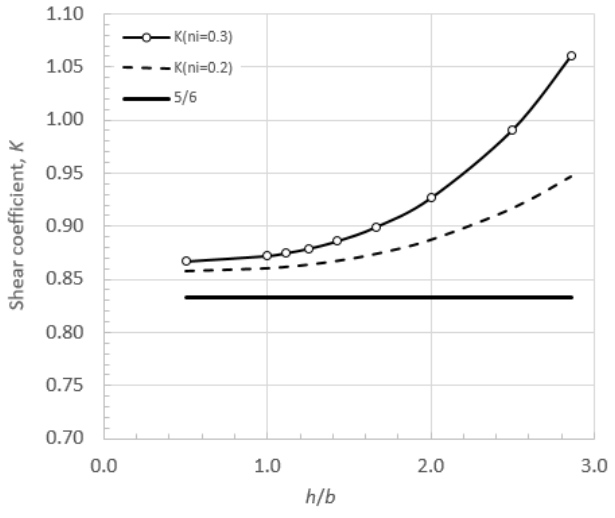
$$S_y(z) = \frac{2}{3}r^3cos^3\beta, dA = b(z)dz = 2r^2cos^2\beta d\beta$$

(25) $$c_{\odot} = \frac{16}{\pi r^6} 2\int_0^{\pi/2} \frac{1}{9}r^4cos^4\beta.2r^2cos^2\beta d\beta = \frac{64}{9\pi}\frac{5}{16}\frac{\pi}{2} = \frac{10}{9} = \frac{1}{k_{\odot}}$$

4. The shear correction factor, according to some authors

There are other suggestions in the literature for these coefficients, which have been obtained when considering hypotheses for a more complex and probably more accurate distribution of the tangential force in the cross-section.

According to Cowper [16], the shear correction factor for rectangular cross-section depends on the Poisson's ratio in conformance with Eq. (26) and for circular cross-section – by Eq. (27).



(26), (27) $$k_{\blacksquare} = \frac{10(1+\nu)}{12+11\nu} \qquad k_{\odot} = \frac{6(1+\nu)}{7+6\nu}$$

Fig. 4. *The shear coefficient for rectangular cross-section depends on the shape (h/b) and on the Poisson's ratio.*

More precise values for the shear correction factor of rectangular and circular cross-sections are suggested by Kaneko [17]:

(28), (29) $$k_{\blacksquare} = \frac{5+5\nu}{6+5\nu} \qquad k_{\odot} = \frac{6+12\nu+6\nu^2}{7+12\nu+4\nu^2}$$

For circular cross-section Stephen [5] gives Eq. (29). However, for rectangular cross-section, the chosen distribution of the stress is more complicated and Stephen obtained a relationship [5] that depends not only on the Poisson's ratio but also from the aspect ratio (h/b , height/width). It is shown in Fig. 4 for two typical values for Poisson's ratio and is compared there with the reference coefficient k = 5/6. According to this relationship, $k_{\blacksquare}$ = 0.860 for material with $\nu = 0.20$ and square cross-section.

5. Conclusion

This article explains a mathematically consistent approach for solving the Equations (4), (5), (6) in Timoshenko's beam theory. It is based on separate integration of both terms in the right side of eq. (4). In this integration, the functions for the bending moment and shear force are used.

Theoretic sections 3.4 - 3.5 give a good description of the shear deformation and the theory for calculating deflections of beams under bending, taking into account both causes for deflection: bending moment and shear force. Fig. 2 visualises the shear-deflection and shear-correction method in a new way.

This work has been started with an aim to check the validity of Eq. (1). An exact solution is not presented here, but we can confirm that the presented here theory leads to this equation for short rectangular beams with shape as specified in the mentioned standards and subjected to four-point bending when a shear correction factor k = 5/6 is accepted.

The Stephen's approach suggests probably more accurate value for mortar and concrete: $k_{\blacksquare}$ = 0.860 for materials with $\nu = 0.20$ and square cross-section.

6. References

1. S.P. Timoshenko, *History of Strength of Materials.* State publ. house for technical-theor. Literat. Moscow. (1957) (in Russian)
2. S.P. Timoshenko, J.N. Goodier, *Theory of Elasticity*. McGraw-Hill Book company Inc, (1951).
3. S.P. Timoshenko *Strength of Materials. Part I. Elementary theory and problems*. Publ. D. van Nostrand company. II ed. (1948)
4. S.P. Timoshenko, Phil. Mag. **41**, 744-746 (1921).
5. N.G. Stephen, J. Appl. Mech. *Mar*., **47** (1): 121-127 (1980)
6. I. Kisiov, *Strength of materials, III ed.* Technika. (1963) (in Bulgarian "Съпротивление на материалите")
7. EN ISO 178:2019. *Plastics – determination of flexural properties*
8. G.M. Gere, B.G Goodno, *Mechanics of materials 8-th ed., SI.* Cengage Learning (2013)
9. S.P. Mandgakov, Mandichev GI, Veselinov KV et. al. *Collection of Problems and Methodological Guidelines on Strength of Materials*. Ed. by S.P Nedelchev. Technika. (1989) (in Bulgarian "СБОРНИК от задачи и методически указания по съпротивление на материалите")
10. K.T. Chan, K.F. Lai, N.G. Stephen, K. Young. J. of Sound and Vibr. **330** (14), pp. 3488-3497 (2011)
11. H. Hadavinia, K. Gordnian, J. Karwatzki and A. Aboutorabi, SDHM, **2** No 4, pp.197-206 (2006)
12. N.G. Stephen, J. of Sound and Vibr. **292**, pp. 372–389 (2006)
13. X.-F. Li, J. of S. and Vibr. **318** No 4-5, pp. 1210–1229 (2008)
14. Jae-Hoon Kang, J. of Sound and Vibr. **333** No 14, pp. 3332–3337 (2014)
15. Marie Brons, J.J. Thomsen, J. of Sound and Vibr. **459**, 114856 (2019)
16. G.R. Cowper, J. Appl. Mech., **33** No 2, pp. 335–340 (1966)
17. T. Kaneko, J. Phys. D (Appl. Phys.) **8,** No 16, pp. 1927-1936 (1975).
18. A. Dı´az-de-Anda, J. Flores, et al., J. of Sound and Vibr. **331,** No 26, pp. 5732–5744 (2012)
19. T.H.G. Megson *Aircraft Structures for engineering students. IV ed*. ELSEVIER (2007)
20. Ke Gong, Appl. Math. and Mech. (Engl. Ed.), **21**, No 9 pp. 1091-1098 (2000)
21. Yuwaraj M.Ghugal, Rajneesh Sharma, Lat. Amer. J. of Solids and Structures, **8,** No 2, pp. 183 – 195 (2011)

Application of artificial locust swarm routing algorithm for VFR flights planning

Vladyslav Alieksieiev[1,2,3], Halyna Ivasyk[1,4], Ivanna Andrusiak[1,5]
[1] Lviv Polytechnic National University, Lviv, Ukraine
[2] RocketRoute Ltd, Farnborough, Hampshire, UK
[3] vladyslav.i.alieksieiev@lpnu.ua, https://orcid.org/0000-0003-0712-0120
[4] halyna.v.ivasyk@lpnu.ua
[5] ivanna.v.andrusyak@lpnu.ua

Abstract: *Along recent years an approach of Artificial Locust Swarm Routing (ALSR) algorithm was developed for flights planning in Europe and for rules provided in EuroControl area of responsibility. Most researches were strictly related to IFR type of flights. However, there is a big area of interest in private aviation for short local flights under the top of VFR flight levels (FL195 and below). These flights have much specificity for planning and ALSR algorithm is found capable of solving these problems also, using this same idea of the algorithm like it was developed for IFR flights. One may see that the algorithm shows rather good results for such difficult area like Swiss Alps valleys and canyons.*
Keywords*: VFR FLIGHT, FLIGHT ALONG CANYON, FLIGHT PLANNING, ROUTING PROBLEM, ALSR ALGORITHM*

1. Introduction

Since invention of word ‘robot’ [1] by Karel Čapek (and Josef Čapek) in 1920, when it was presented in his play “Rossum's Universal Robots”, the mankind had many achievements in development of robots. Now, after less than 100 years the ideas of fourth industrial revolution [2], smart factories, autonomous production, and autonomous machines are nearly implemented. However, there is still much left to discover in the area. Nevertheless, those fictional humanoids from Čapek’s play and named robots, nowadays look not so fictional ones. Among those research areas giving life to modern autonomous and semi-autonomous robots there is an orientation in space and path finding. If one would like to build and exploit a fleet of flying robots, or ‘drones’, for the purpose of manufacturing [3] or environment surveillance [4], then those drones should inevitably be capable of finding path between two points (departure and destination) in any space. And for sure it becomes very beneficial that someone already invented some algorithm for the path finding problem [5-9]. So, the drone may choose to simply use the shortest path algorithm or the algorithm to avoid obstacles on its way and how to consider the airspace it operates in [10-12]. It is worth mentioning that a huge boost to development in this area was given by Marco Dorigo and his natural algorithm approach [13-14]. Many of so-called nature-inspired algorithms could be considered inspired by success of his now well-known ant algorithm. Among these nature-inspired algorithms one may find ABC (artificial bee colony) [15], BNMR (blind, naked mole-rats) [16], GOA (grasshopper optimization algorithm) [17], ALSR (artificial locust swarm routing) [18-20], and many others.

However, most known path search algorithms are developed to serve on a topology that could be presented with a graph (even a planar graph). Typically, such algorithm and their implementations require having a predefined graph topology. Unlike to those approaches, the focus of this paper is on ALSR algorithm which implies being free of predefined graph topology. It is implemented here to VFR flight path search problem. Now we are to discuss some algorithm issues for the VFR flight planning and possible ways to overcome these issues.

2. Prerequisites and means for solving the problem

First, lets unveil the meaning of VFR flight planning problem. The VFR stands for ‘visual flight rules’. According to IFPS User Manual by EuroControl [21] the VFR flight could be performed at a good weather conditions on lower flight levels (typically below FL195) and often close to the terrain. In particular, we were investigating the case when the VFR flight should be performed in mountainous area (Alp mountains) along the canyon. The flight between LSMM (Meiringen, Switzerland) and LSZB (Bern, Switzerland) airports allows to search for a path along the canyon. The flight between LSZB (Bern, Switzerland) and LIPQ (Trieste, Italy) allows to consider flight through/around Alp mountains.

Second, the data given for a VFR flight may contain one of the following limitations at bottom level:

- grid MORA (minimum off-route altitudes),
- terrain elevation.

It is worth mentioning here, that grid MORA could give rather high flight level for a wide area above the terrain. This means that aircraft may fly safely without danger of crashing the ground or hitting the mountain. Unlike to this case, the terrain elevation could be a very realistic case for the crash due to proximity of the ground. While the full dataset of terrain elevations is huge, we make an assumption that the terrain could be divided into ‘squares’ (0.5NM side) and each whole square has elevation of its center point (this grid could be something similar to grid MORA, but more detailed).

Third, the VFR flight considers points, both published points (in Europe these points come in AIXM format [22]) and VRPs (visual reference points – landmarks used for position reporting by aircraft, typically some objects that could be visibly recognized by pilots).

One may find VFR flight planning in some way similar to FRA flight planning, while there are no airways and direct segment (DCT) should connect two consecutive points on a route. However, the FRA (free route airspace) [23] is defined high above terrain and has no danger of collision with the ground above the bottom of the FRA.

3. Solution of the examined problem

Let’s consider first the case of grid MORA and implementation of ALSR algorithm for path search in this case (Fig. 1 and Fig.2).

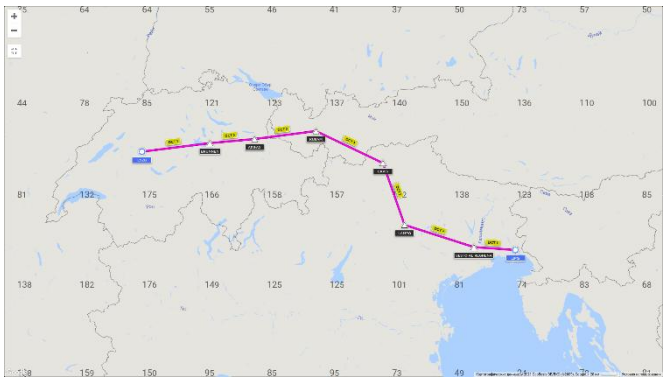


Fig. 1 *Path search with ALSR algorithm between LSZB and LIPQ airports: maximum DCT length 50NM and maximum FL 150.*

We search for the route from LSZB (Bern, Switzerland) to LIPQ (Trieste, Italy). The ALSR algorithm was provided with VRPs additionally to normal published points (both designated points and navaid points from AIXM data) and grid MORA to

define a bottom level for the flight. At Fig.1. the maximum allowed length for DCT was set to 50NM and at Fig.2 there is a maximum allowed DCT length set to 30NM.

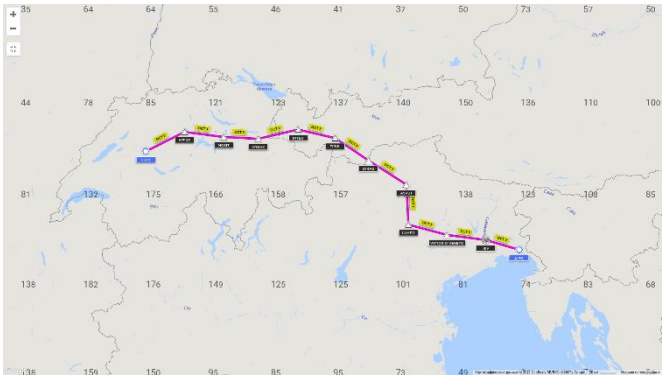


Fig. 2 *Path search with ALSR algorithm between LSZB and LIPQ airports: maximum DCT length 30NM and maximum FL 150.*

As one can see, both routes (Fig.1 and Fig.2) were found to go around Alp mountains. This case revealed ALSR algorithm ability to easily connect two airports and didn't require any serious modifications to the code. This case looks more like a FRA route.

Next, let's see what happens in behavior of the ALSR algorithm for the case of terrain elevation used as a bottom level for the flight. The terrain elevation was defined within the grains ('squares') of 0.5NM×0.5NM. And cap for the flight was set to FL35 (see Fig.3).

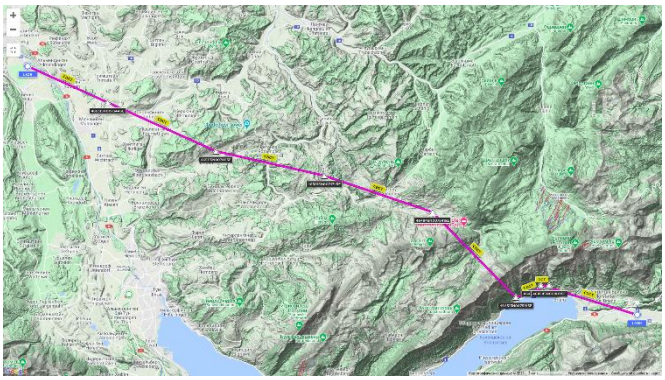


Fig. 3 *Path search with ALSR algorithm from LSMM to LSZB airport: maximum DCT length 5NM and maximum FL 35.*

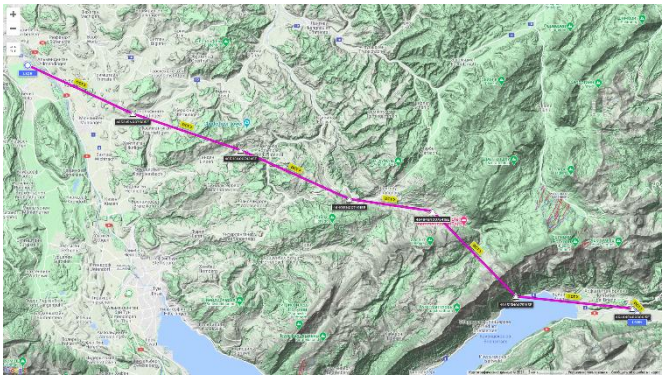


Fig. 4 *Path search with ALSR algorithm from LSZB to LSMM airport: maximum DCT length 5NM and maximum FL 35.*

Analysis of the route at Fig.3 and Fig.4 revealed that route was built successfully (into both directions), however, the length of the DCT allows to jump over the mountain, which could be higher, than the maximum allowed level. So, the more detailed consideration of each DCT should be added. However, if the data for the grain center point (used as a grid point) does not consider maximum terrain elevation within the grain, then route may also 'hit the mountain'. This means the data of terrain elevations should be prepared very carefully. Unfortunately, the detailed consideration of each segment makes negative impact on time, that is consumed to find a route.

It is also should be mentioned here that now there are too many points available for search of path between departure and destination airports, unlike to case with published points. It is both absolutely unrealistic and quite useless to consider the whole globe with terrain elevations at each square. The important step for the ALSR algorithm here is to cut only the relevant airspace area [24]. This approach was successfully used to reduce number of excessive points.

The interesting question was whether ALSR algorithm is capable of finding path along the canyon. As one can see at Fig.5 and Fig.6 the algorithm revealed some 'rush state'. This means before the route becomes smooth and leads to destination, it dashes aside to the points, which are considered closer to the destination, and fail to continue except going somewhere back. Despite of connecting departure and arrival airports, the route cannot be used for flight planning. Hence, the algorithm should be corrected to remove such 'rush state' at initial stage of route.



Fig. 5 *Path search with ALSR algorithm from LSMM to LSZB airport: maximum DCT length 5NM and maximum FL 25.*

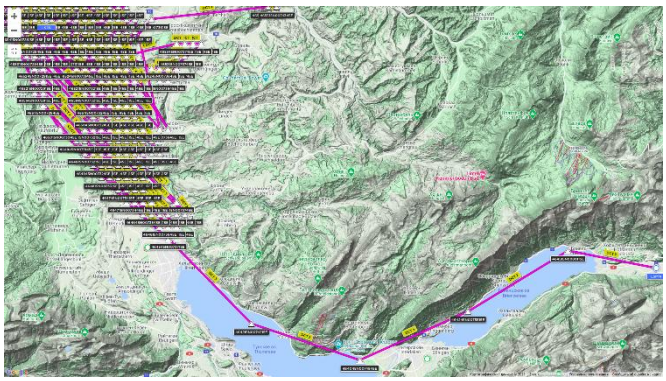


Fig. 6 *Path search with ALSR algorithm from LSZB to LSMM airport: maximum DCT length 5NM and maximum FL 25.*

The solution for the problem was found in forbidding the algorithm to make sharp turns, like turns back. This really solves the problem, because the route becomes smooth without dashes aside. This could be explained by fact, that attempts in a 'wrong' direction now fail and are not allowed to be used to continue. The results are presented at Fig.7 and Fig.8. The interesting thing is, that all those changes applied in algorithm made it find routes along canyon not only at FL25, but also at FL35, which was not observed before.

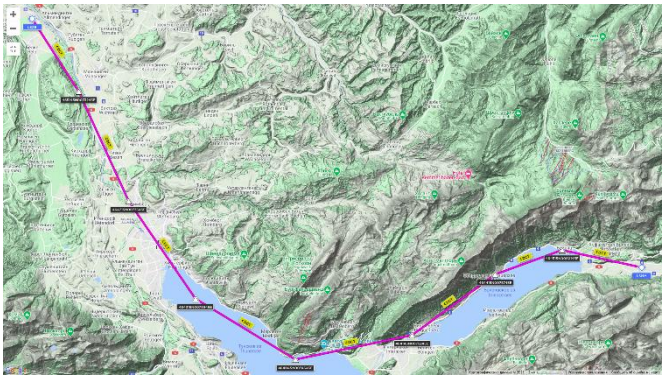


Fig. 7 *Path search with ALSR algorithm from LSMM to LSZB airport: maximum DCT length 5NM and maximum FL 25.*

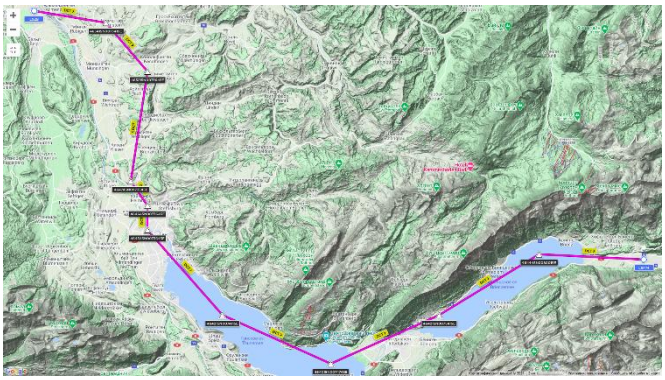


Fig. 8 *Path search with ALSR algorithm from LSZB to LSMM airport: maximum DCT length 5NM and maximum FL 25.*

4. Results and discussion

A custom software solution for the algorithm was developed using Microsoft Visual Studio 2015 in C++ programming language. Currently, an initial test of a locust swarm algorithm for solving routing problem was made as a plain routing with randomly generated topologies. Simulations were performed on a Dell Inspirion notebook (model no. 3737-5683) with Intel Core i7 processor. The results were visualized using RocketRoute Flight Planning Center [25].

The Artificial Locust Swarm Routing (ALSR) algorithm in case of VFR flight with terrain elevation grid was found vulnerable to:

- processing huge dataset of grid points – becomes very time consuming when working with hundreds of thousands of points,
- very detailed consideration of DCT – becomes more time consuming to avoid collision with mountains,
- 'rush state' at initial stage – makes many unnecessary attempts to approach destination point and then stepping in backward direction.

Fortunately, these problems were solved successfully with the following modifications of ALSR algorithm (these same changes are expected to be valid also for IFR/VFR flight with ATS network):

1. Cutting the working area to search for path within relevant area of airspace.
2. Limiting possible turns for the next step to less than 85 degrees (preventing sharp turns and turns into backward direction).

Experimenting with maximum allowed DCT length revealed the following behavior (which could be considered also as expected):

- Shorter DCTs provides more curved path, but it requires more frequent points locations (some points could be located at distance, which is longer than maximum allowed DCT length, and this may cause to either a bad route or a failed routing).
- Longer DCTs may cause a very unsmooth route line, which could be less optimal by distance (however, the route often could be found faster).

While the algorithm showed good results for VFR flights with grid MORA bottom limit, the result with terrain elevation as a bottom limit had some concerns and drawbacks (mostly because of quality and quantity of data). Different attempts revealed ability of ALSR algorithm to connect departure and arrival airport. However, much attention should be paid to ratio of maximum allowed DCT length and distances between points within grid (especially in case of terrain elevation grid).

5. Conclusion

The problem of VFR flights planning was considered and ALSR algorithm implementation was investigated and discussed. Some vulnerabilities and issues of the algorithm were found, and solutions for the problems were offered. The changes made to the algorithm revealed its capability to steadily solve the core problem of connecting two airports (departure and destination). Two cases of defining bottom limit for VFR route were considered according to difference in datasets. For both cases the results were found satisfactory.

While there was found a significant growth of time consumed for path search in case of terrain elevation grid, one may choose to make a precalculated routes and store them into database for further use. On practice it is a rare situation that terrain profile can change frequently from time to time. This means, the route can be re-used effectively from database (with respect to type of flying vehicle and its characteristics). Hence, some particular and independent algorithm for further increase of accuracy or more detailed path analysis can be developed. It can be applied later to a stored route which was generated with ALSR.

The ideas and techniques of flight planning for VFR can be widely used in planning drone flights. However, instead of pilot eyes there could be used sets of sensors. Also, the 'visual' sense for the drone can be enhanced with AI for ground objects recognition.

6. Acknowledgement

RocketRoute Limited (Farnborough, Hampshire, United Kingdom) sponsored the whole research, including current problem analysis and a developed algorithm of an artificial locust swarm routing (ALSR). This research results and all rights for the objects of intellectual property will belong to RocketRoute Limited (Farnborough, Hampshire, United Kingdom).

7. Literature

1. Thomas R. Kurfess, Robotics and Automation Handbook. – CRC Press, 2018. – 608 p.
2. K. Schwab, The Fourth Industrial Revolution. – NY: Crown Publishing Group, 2016 (2017). – 192 p.
3. An approach of FRA and its use for UFV supported manufacturing / V. Alieksieiev, B. Liubinsky, V. Hladun // "Machines. Technologies. Materials." – Scientific-Technical Union of Mechanical Engineering "Industry 4.0" (Sofia, BULGARIA), 2019 – Volume 13, Issue 10. – P.437–438. — https://stumejournals.com/journals/mtm/2019/10/437.
4. Implementation of UAV for environment monitoring of a Smart City with an airspace regulation by AIXM-format data streaming / Vladyslav Alieksieiev, Bohdan Markovych // "Industry 4.0" – Scientific-Technical Union of Mechanical Engineering "Industry 4.0" (Sofia, BULGARIA), 2020 –

Volume 5, Issue 2. – P.90–93. — https://stumejournals.com/journals/i4/2020/2/90.
5. E.W. Dijkstra, “A note on two problems in connexion with graphs”, Numerische Mathematik, Vol. 1, Iss. 1, pp. 269–271 (1959)
6. P.E. Hart, N.J. Nilsson, B. Raphael, “A Formal Basis for the Heuristic Determination of Minimum Cost Paths”, IEEE Transactions on Systems Science and Cybernetics SSC4 (2), pp. 100–107 (1968)
7. H. Berliner, “The B* tree search algorithm. A best-first proof procedure”, Artificial Intelligence, Vol. 12, Iss. 1, pp. 23–40 (1979)
8. A. Stentz, “Optimal and Efficient Path Planning for Partially-Known Environments”, IEEE International Conference on Robotics and Automation, vol. 4, pp. 3310–3317 (1994)
9. R.J. Szczerba, D.Z. Chen, J.J. Uhran Jr. “Planning shortest paths among 2D and 3D weighted regions using framed-subspaces”, The International Journal of Robotics Research, Vol. 17, No. 5, 1998, pp. 531–546.
10. J.O. Royset, W.M. Carlyle, R.K. Wood, “Routing military aircraft with a constrained shortest-path algorithm”, Military Operations Research, Vol. 14, No. 3, 2009, pp. 31–52.
11. Shijin Wang, Xi Cao, Haiyun Li, Qingyun Li, Xu Hang, Yanjun Wang, “Air route network optimization in fragmented airspace based on cellular automata”, Chinese Journal of Aeronautics, No. 30 (3), 2017, pp. 1184–1195.
12. C. K. Jensen, M. Chiarandini, K. S. Larsen, “Flight planning in free route airspaces”, 17th Workshop on Algorithmic Approaches for Transportation Modelling, Optimization, and Systems (ATMOS 2017), 2017 – 14 p.
13. M. Dorigo, “Optimization, Learning and Natural Algorithms”, PhD thesis, Politecnico di Milano, Italy, 1992.
14. M. Dorigo, G.A. Di Caro, L.M. Gambardella, “Ant Algorithms for Discrete Optimization”, Artificial Life, vol. 5, pp. 137–172 (1999)
15. D. Karaboga, B. Basturk, “A Powerful and Efficient Algorithm for Numerical Function Optimization: Artificial Bee Colony (ABC) Algorithm”, Journal of Global Optimization, Vol. 39, No. 3, pp. 459–471 (2007)
16. A novel meta-heuristic algorithm for numerical function optimization: Blind, naked mole-rats (BNMR) algorithm / Mohammad Taherdangkoo, Mohammad Hossein Shirzadi, and Mohammad Hadi Bagheri. // Scientific Research and Essays – Vol. 7 (41), Oct. 2012 – P. 3566-3583 – Retrieved from: https://academicjournals.org/journal/SRE/article-full-text-pdf/F02820F28755
17. Grasshopper Optimisation Algorithm: Theory and application / Saremi S., Mirjalil S., Lewis A. // Advances in Engineering Software – Vol. 105, Mar. 2017 – P.30-47
18. Air space routing and flights planning: a problem statement and discussion of approaches to solution / V. Alieksieiev // “Mathematical Modeling” – Scientific-Technical Union of Mechanical Engineering “Industry 4.0” (Sofia, BULGARIA), 2018 – Volume 2, Issue 4 – P.139–142. — https://stumejournals.com/journals/mm/2018/4/139.
19. V. Alieksieiev, “Artificial Locust Swarm Routing Algorithm: An Approach to Consider both Routing via FRA and Applying RAD”, 2019 International Conference on Information and Digital Technologies (IDT), 2019, pp.1-10. — https://ieeexplore.ieee.org/document/8813465.
20. V. Alieksieiev, A. Berko, “Artificial Locust Swarm Routing Algorithm: Decision Making in Path Search Problem”, 2019 11th International Conference on Electronics, Computers and Artificial Intelligence (ECAI), 2019, pp.1-6. — https://ieeexplore.ieee.org/document/9041925.
21. IFPS User Manual – EUROCONTROL, 2019 – https://www.eurocontrol.int/sites/default/files/2019-05/ifps-users-manual-current.pdf.
22. Aeronautical Information Exchange Model – http://aixm.aero
23. Free route airspace (FRA) – Eurocontrol, https://www.eurocontrol.int/articles/free-route-airspace.
24. The approach to cut relevant airspace area for flights planning and automated routing / V. Alieksieiev, I. Alieksieiev // “Industry 4.0” – Scientific-Technical Union of Mechanical Engineering “Industry 4.0” (Sofia, BULGARIA), 2019 – Volume 4, Issue 5. – P.220–222. — https://stumejournals.com/journals/i4/2019/5/220.
25. Flight Planning Centre RocketRoute – https://fly.rocketroute.com.

Automated system of getting meter readings in the sphere of communal services

Volodymyr Hladun[1,2], Bohdan Liubinsky[1,3] Petro Topylko[1,4]

[1] Lviv Polytechnic National University, Lviv, Ukraine

[2] volodymyr.r.hladun@lpnu.ua, https://orcid.org/ 0000-0002-4337-8869
[3] bohdan.b.liubinsky@lpnu.ua, https://orcid.org/0000-0002-0715-8068
[4] petro.i.topylko@lpnu.ua, https://orcid.org/0000-0002-8634-0588

Abstract: *The work demonstrates the implementation of automated meter data reading using a single-board computer Raspberry Pi model 3B +, camera module. The approach of creation of the UWP-application and the Web API as a server part is considered.*

Keywords*: AUTOMATED SYSTEM, METER READING, MUNICIPAL UTILITIES, RASPBERRY PI,*

1. Introduction

The main reason for the development of automatic transmission of data on utilities was unstable and untimely reporting of consumed utilities to Ukraine's corresponding institutions. The majority of consumers regularly face overpayments in municipal services almost every month, which is associated with the forecast amount of resources used by the resident for a given month. There's also a possible opposite case when the approximate added volume is less than consumed and after presenting the true values you may face a large debt at the end of the month. The main cause for these situations is the late submission of meter readings within the specified period. According to the rules of the retail market of water, electricity, and gas, a consumer is obliged to take monthly readings of the meter as of the 1st and within five calendar days either by providing them in SMS or calling the appropriate system operator or by record submission in their personal account online. This process can be automated by creating an automated meter reading system. To approach this, it's been proposed to take meter readings, then capture them at regular intervals, and eventually, send data to the appropriate organizations. This solution could facilitate the process of submitting indicators and help to avoid debts during the payment period for utilities.

The main device of the automated system of receiving the image of indicators of the counter is Raspberry PI [1,2]. The following frameworks and technologies have been used in this work:

- *Xamarin.Forms* is a platform[3] for creating applications that work with hardware platforms for Android, iOS, and Windows 10. The framework is designed based on the MVVM template
- *Prism framework* for building[5,7] free-coupled, maintained, and tested XAML applications in WPF, Windows 10 UWP, and Xamarin Forms.
- *Object* of HttpClient class for passing[6] the HTTP requests.
- *Web API* for application[4] programming.
- *MVC framework* for building the server part[4] of the application architecture
- *Image recognition technology*

2. Software architecture requirements

The following functional requirements have been collected to build a UWP-application as a client part and a web service:

I. The UWP-application must access the connected camera module.

II. The UWP-application must take a photo of the meter at regular intervals

III. The UWP-application must prepare the data for transmission to Web API

IV. The UWP-application must leverage the data transfer protocol - HTTP. This is necessary to fulfill the restrictions imposed by REST API

V. The UWP-application must send data in JSON format

VI. The web service must retrieve text from the submitted image.

VII. The web service must send the recognized text to Gmail.

VIII. Collected functional requirements for UWP-application and web service fully satisfy the software architecture

You can find the UML architecture diagram as shown below (see Figure 1):

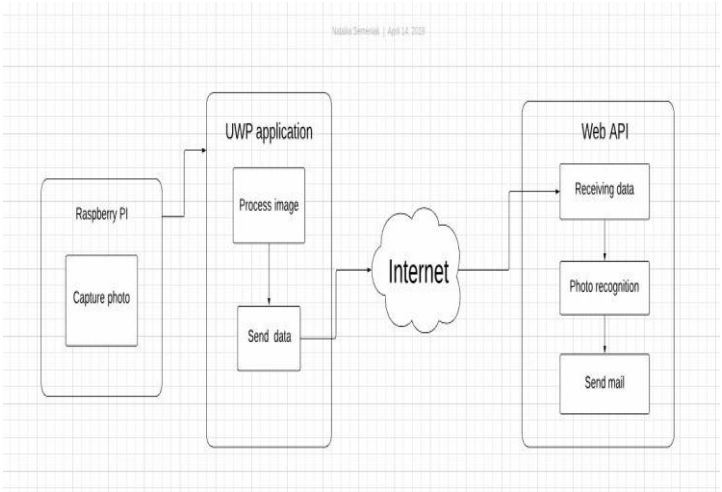


Fig. 1 *UML architecture diagram*

The main modules of architecture include:

- Raspberry PI configuration module
- Meter readout module
- Meter transmission module
- Receiving sent data module
- Picture recognition module
- Data sending module

3. Automated system: economic justification

This work leverages a Raspberry PI microcomputer, with an average price of UAH 1,300. A webcam (UAH 250-300) has been used to get the picture. Therefore, the estimate of this project would be the maximum price of UAH 1,600.

A budget option is possible after the Raspberry PI [1,2,8] replacement by Aurduino microcontroller (at the price 400-500

UAH). However, the Raspberry PI can be called a full-fledged computer, which isn't the case with the Aurduino. The Raspberry PI is 40 times faster than the Arduino. An even bigger gap in RAM: The Raspberry PI has 128,000 times more RAM than the Arduino. Raspberry PI is a computer that can be run a multitasking-support operating system. In turn, the Arduino is better able to read analog signals in real-time. This flexibility allows the Arduino to work with virtually any type of sensor or chip.

To solve this problem from a software perspective, it'd have been more profitable to work with Raspberry PI for less time, but more cost-effective in comparison to Arduino

4. Conclusion

In this paper, we've reviewed the current problem for Ukraine - the meter readings delivery. The technologies used to create, recognize and send data are analyzed. The specification of requirements for software architecture is collected. The architecture of the automated meter reading system is constructed. We've also provided the economical justification of such a system usage.

5. Literature

1. Matt Richardson, Shawn Wallace. Getting started with Raspberry PI. - Maker Media, Inc, 2003. - 176 c.
2. Agus Kurniawan Getting Started with Windows 10 IoT Core for Raspberry PI 3. - PE Press; 06. 30, 2016. - 113 c.
3. Charles Petzold. Creating Mobile Apps with Xamarin.Forms.- Redmond, Washington, 2014. - 1149 c.
4. Create a Web API with ASP.NET Core MVC - https://docs.microsoft.com/en-us/aspnet/core/tutorials/first-web-api?view=aspnetcore-2.2&tabs=visual-studio.
5. Image Recognition and Object Detection: Part 1 - https://www.learnopencv.com/image-recognition-and-object-detection-part1/.
6. HttpClient Class - https://docs.microsoft.com/en-us/dotnet/api/system.net.http.httpclient?view=netframework-4.8.
7. Prism documentation - URL: http://prismlibrary.github.io/docs/.
8. Raspberry PI documentation - https://www.raspberrypi.org/.

A new Approach to Modeling and Simulation of Industrial Processes

Christo Boyadjiev
Institute of Chemical Engineering,
Bulgarian Academy of Sciences, Bulgaria
E-mail: chr.boyadjiev@gmail.com

Abstract. *In the paper are presented theoretical analysis of the methods for industrial processes modeling and a new approach to modeling and simulation of industrial processes in cases of lack of information on the mechanism of the process.*
KEYWORDS: *MODELING, SIMULATION, CHEMICAL ENGINEERING, INDUSTRIAL PROCESSES*

Prelude

The main problems in the industry are the optimal design of new devices and the optimal control of active processes, i.e., minimization of the investment and operating costs. These problems are solved by modeling methods [1].

The creation of the mathematical model begins with the formulation of the physical model of the complex process, i.e., the definition of the simple (elementary) processes that make it up and the interactions between them. The second step is to define simple processes that have mathematical descriptions (equivalent mathematical operators). The other simple processes are introduced into the mathematical model through quantitative information obtained from experimental data, which brings the mathematical model as close as possible to the real process. The experiment brings mathematics closer to physics (reality).

The optimal design and control in the chemical industry is uniquely related to processes rates, so all mathematical descriptions of processes are linked to algorithms to determine these rates, i.e., processes kinetics.

Industrial Processes Kinetics

The industrial systems consist of separate phases (gas, liquid, solid) in the industrial apparatuses volumes. They are in thermodynamic equilibrium when the temperatures and concentrations of substances in the individual parts or points of the phases are equal and the velocities are equal to zero.

The processes in the industry are a result of the deviation of the systems from their thermodynamic equilibrium [2]. One system is not in a thermodynamic equilibrium when the velocities, concentrations of the components (substances) and the temperatures at the individual points in the phase volumes are different. These differences are the result of reactions, i.e., of processes that create or consume substance and (or) heat. As a result, the industrial processes kinetics is equivalent to the reactions kinetics [3].

The presented analysis shows that processes in the industry are result of reactions that occur in the phase volume (homogeneous) or on the boundary between two phases (heterogeneous). Homogeneous reactions are generally chemical, while heterogeneous reactions are chemical, catalytic, physical and chemical adsorption, interphase mass transfer in gas-liquid and liquid-liquid systems (on the interphase surface the substance disappears from one phase and occurs in the other phase). The rates of these processes are determined by the reaction kinetics [3], which lies at the basis of modeling and simulation of the industrial processes.

Modeling

The basics of modeling in chemical engineering, as part of human knowledge and science, are related to the combination of intuition and logic that has different forms in individual sciences [4]. In the mathematics the intuition is the axiom (unconditional statements, that cannot be proven), while the logic is the theorem (the logical consequences of the axiom), but logic prevails over intuition. In the natural sciences (physics, chemistry, biology), the "axioms" (principles, postulates, laws) are not always unconditional, but logic prevails over intuition too.

The processes in the industry take place in the industrial apparatuses, where gas, liquid and solid phases move together or alone. They are described by variables, which are extensive or intensive. In the case of merging of two identical systems, the extensive variables are doubled, but the intensive variables are retained.

In the industry, processes take place in moving phases (gas, liquid, solid). Reactions (reaction processes) lead to different concentrations (and temperatures) in the phase volumes and the phase boundaries. As a result, hydrodynamic processes, diffusion mass transfer and heat conduction are joined to the reaction processes. Under these conditions there are various forms of mass transfer (heat transfer) that are convective (as a result of phase movements) and diffusion (as a result of concentration (temperature) gradients in the phases).

Convective mass transfer (heat transfer) can be laminar or turbulent (as a result of large-scale turbulent pulsations). Diffusion mass transfer (heat transfer) can be molecular or turbulent (as a result of small-scale turbulent pulsations).

Mathematical models of industrial apparatuses aim at determining the concentration of substances (flow temperatures) in the phases. They have different degrees of approximation – thermodynamic, hydrodynamic and Boltzmann's approximations.

Thermodynamic Approximation

The processes in chemical engineering are result of a deviation from the thermodynamic equilibrium between two-phase volumes or the volume and phase boundaries of one phase and represent the pursuit of systems to achieve thermodynamic equilibrium [2]. They are irreversible processes and their kinetics use mathematical structures derived from Onsager's principle of linearity (axiom). According to him, the average values of the derivatives at the time of the extensive variables depend linearly on the mean deviations of the conjugated intensive variables from their equilibrium states. The principle is valid close to equilibrium, and the Onsager's linearity coefficients are kinetic constants. When the process is done away from equilibrium (high intensity processes) kinetic constants become kinetic complexes, depending on the corresponding intensive variables. The thermodynamic approximation models cover the entire volume of the phase or part of it.

Hydrodynamic Approximations

The hydrodynamic level uses the approximations of the mechanics of continua, where the mathematical point is equivalent to an elementary physical volume, which is sufficiently small with respect to the apparatus volume, but at the same time sufficiently large with respect to the intermolecular volumes in the medium. In this level the molecules are not visible, as is done in the next level of detail of Boltzmann.

The models of the hydrodynamic approximations are possible to be created on the basis of the mass (heat) transfer theory, whose models are created by the models of the hydrodynamics, diffusion, thermal conductivity and reaction kinetics, using the logical structures of three main “axioms”, related with the impulse, mass and heat transfer:

1. The postulate of Stokes for the linear relationship between the stress and deformation rate, which is the basis of the Newtonian fluid dynamics models;
2. The first law of Fick for the linear relationship between the mass flow and the concentration gradient, which is the basis of the linear theory of the mass transfer;

3. The first law of Fourier for the linear relationship between the heat flux and the temperature gradient, which is the basis of the linear theories of the heat transfer.

These are the laws of the impulse, mass and energy transfer.

To the above axioms must be added the law of chemical kinetics - the rate of two-molecular reactions depends linearly on the product of the concentrations of the reagents. This law is not an axiom because it follows from the rule of probabilities. The reaction between two molecules takes place when they are at one point. The probability that a molecule of a reagent is at a given point is equal to the ratio of the number of its molecules and the total number of molecules, i.e, it is proportional to its concentration. The same is true for the second reagent. The simultaneous realization of both probabilities is the complex probability, which is equal to the product of the simple probabilities.

Boltzmann's Approximation

In Boltzmann's kinetic theory of the ideal gas, the hydrodynamic "axioms" are three "theorems" that derive from the axiom of the "elastic shock" (in a shock between two molecules the direction and the velocity of the movement change, but the sum of their kinetic energies is retained, i.e., there is no loss of kinetic energy) and the rate coefficients are theoretically determined by the average velocity and the average free run of the molecules.

Mechanism of Influence of Reaction Kinetics

The mathematical model of an engineering process is a mass (heat) balance in the phases volumes, where the mathematical operators are mathematical descriptions of the composite (elementary) processes, and the relationship between them (differential equations) corresponds to the mechanism of the complex process. The boundary conditions of the differential equations are formulated at the interphase boundaries.

Industrial processes are a set of physical and chemical reactions, hydrodynamic, diffusion and thermal processes that take place in the industrial apparatus volume. The problems in the modeling of the kinetics of industrial processes arise from the need for information about the interaction between the simple (elementary) processes in the complex process, i.e., information about the process mechanism.

Modeling of Processes with Unknown Mechanism

There are complex processes whose mechanism is unknown. A typical example of this are the complex chemical reactions, where the rate of which depends on the concentrations of several substances, but the simple chemical reactions between these substances and the relationships between them are unknown.

The kinetics of processes with an unknown mechanism can be modeled on the basis of an axiom, which can be formulated as it - "The mathematical structure of the quantitative description of real (industrial) processes does not depend on the measuring system of the quantities involved in them".

A. A. Gukhman formulates [8] the condition for homogeneity of a function – „The function in the equation $F\left(x_1,...,x_n\right)=0$ is homogeneous, if is invariant $F\left(k_1x_1,...,k_nx_n\right)=0$ with respect to similar transformations $x_i=k_ix_i, i=1,...,n$ ($k_i, i=1,...,n$ - positive constants)", i.e.,

$$F\left(k_1x_1,...,k_nx_n\right)=\varphi\left(k_1,...,k_n\right)F\left(x_1,...,x_n\right). \quad (1)$$

The homogeneous functions satisfy the equation (1) in the cases $F\left(x_1,...,x_n\right)\neq 0$, too.

Using the equation (1), Gukhman formulates and proves the theorem [5] – "If mathematical structure is invariant with respect to similar transformations, it is possible to be presented as power functions complex". This Gukhman's theorem can be considered as a consequence of the axiom „Mathematical structure of real process does not depend on the measuring system", because the mathematical structure, which is invariant with respect to similar transformations is mathematical structure of real processes, which does not depend on the measuring system. As a result is possible to be formulate the theorem „Mathematical structure of the quantitative description of real systems is possible to be presented as power functions complex". This theorem will be proved for cases of complex chemical reactions.

The kinetics of the complex chemical reactions depends on a set of variables. If the velocity of these processes is denoted by y and the values of these variables are $x_1,...,x_n$, the equation of the kinetic model will have the form:

$$y=f\left(x_1,...,x_n\right). \quad (2)$$

This function is a mathematical structure that is retained when changed the measurement system of the variable, i.e., this mathematical structure is invariant with respect to similar transformations [5]:

$$\overline{x}_i=k_ix_i, \quad i=1,...,n, \quad (3)$$

i.e., f is a homogeneous function:

$$ky=f\left(k_1x_1,...,k_nx_n\right)=\phi\left(k_1,...,k_n\right).f\left(x_1,...,x_n\right), \quad k=\phi\left(k_1,...,k_n\right). \quad (4)$$

A short recording of (4) is:

$$f\left[\overline{x}_i\right]=\phi\left[k_i\right]f\left[x_i\right]. \quad (5)$$

The problem consists in finding a function *f* that satisfies equation (5). A differentiation of equation (5) concerning k_1 leads to:

$$\frac{\partial f\left[\overline{x}_i\right]}{\partial k_1}=\frac{\partial \phi}{\partial k_1}f\left(x_i\right). \quad (6)$$

On the other hand

$$\frac{\partial f\left[\overline{x}_i\right]}{\partial k_1}=\frac{\partial f\left[\overline{x}_i\right]}{\partial \overline{x}_1}\frac{\partial \overline{x}_1}{\partial k_1}=\frac{\partial f\left[\overline{x}_i\right]}{\partial \overline{x}_1}x_1. \quad (7)$$

From (6, 7) follows

$$\frac{\partial f\left[\overline{x}_i\right]}{\partial \overline{x}_1}x_1=\alpha_1\ f\left[x_i\right], \quad (8)$$

where

$$\alpha_1=\left(\frac{\partial \phi}{\partial k_1}\right)_{k_i=1}. \quad (9)$$

The equation (8) is valid for different values of k_i including $k_i=1\ \left(i=1,...,n\right)$. As a result $\overline{x}_i=x_i, i=1,...,n$ and from (8) follows

$$\frac{1}{f}\frac{\partial f}{\partial x_1}=\frac{\alpha_1}{x_1}, \quad (10)$$

i.e.

$$f = c_1 x_1^{\alpha_1}. \quad (11)$$

When the above operations are repeated for $x_2,...,x_n$, the homogenous function *f* assumes the form:

$$f = k x_1^{\alpha_1},...,x_n^{\alpha_n}, \quad (12)$$

i.e. the function *f* is homogenous if it represents a power functions complex and as a result is invariant with respect to similarity (metric) transformations. The parameters $k,\alpha_1,...,\alpha_n$ are determined by experimental data of the industrial process velocity.

Parameters Identification

The parameters $k,\alpha_1,...,\alpha_n$ identification in (12) uses experimental data of the industrial process velocity $f_j^{\exp}$, $j=1,...,N$ for different values of the variables are $x_{1j},...,x_{nj}$, $j=1,...,N$, where the calculated values of the industrial process velocity are

$$f_j = k x_{1j}^{\alpha_1},...,x_{nj}^{\alpha_n}, \quad j=1,...,N. \quad (13)$$

The parameters identification of the model requires its preliminary logarithmization

$$F_j = \alpha_0 + \alpha_1 X_{1j},...,\alpha_n X_{nj}, \quad j=1,...,N, \quad F=\log f, \quad \alpha_0 = \log k, \quad X = \log x \quad (14)$$

The differences between the calculated and experimental values of the industrial process velocity will be presented as

$$\alpha_0 + \alpha_1 X_{1j},...,\alpha_n X_{nj} - F_j^{\exp} = \varepsilon_j, \quad j=1,...,N, \quad F_j^{\exp} = \log f_j^{\exp} \quad (15)$$

.

The solution of the parameters identification problem can be obtained as a minimization of the least-squares function:

$$Q(\alpha_0,\alpha_1,...,\alpha_n) = \sum_{j=1}^{N}\left(\alpha_0 + \alpha_1 X_{1j},...,\alpha_n X_{nj} - F_j^{\exp}\right)^2, \quad (16)$$

using the condition

$$\frac{\partial Q}{\partial a_i} = 0, \quad i = 0,1,...,n \quad , (17)$$

i.e.

$$\sum_{j=1}^{N} 2\left(\alpha_0 + \alpha_1 X_{1j},...,\alpha_n X_{nj} - F_j^{\exp}\right) = 0,$$

$$\sum_{j=1}^{N} 2\left(\alpha_0 + \alpha_1 X_{1j},...,\alpha_n X_{nj} - F_j^{\exp}\right) X_{1j} = 0,$$

$$\sum_{j=1}^{N} 2\left(\alpha_0 + \alpha_1 X_{1j},...,\alpha_n X_{nj} - F_j^{\exp}\right) X_{2j} = 0, , \quad (18)$$

...

$$\sum_{j=1}^{N} 2\left(\alpha_0 + \alpha_1 X_{1j},...,\alpha_n X_{nj} - F_j^{\exp}\right) X_{nj} = 0.$$

The solution of the equation set (18) permits to be obtained the parameters values in the model (12). Determining parameter $\kappa = 10^{\alpha_0}$ by antilogarithmization of parameter α_0 is not recommended due to increasing computational error of α_0. The equation (13) can be used for this purpose:

$$k = \frac{1}{N}\sum_{j=1}^{N} \frac{f_j}{x_{1j}^{\alpha_1},...,x_{nj}^{\alpha_n}}. \quad (19)$$

Presented algorithm (13-19) permits to use power functions complex (12) as an universal model of the real (industrial) processes.

Conclusions

In the paper is presented a theoretical analysis of the methods for industrial processes modeling.

The role of the kinetics of industrial processes for solving the problems of optimal design and control is analyzed. The thermodynamic, hydrodynamic and Boltzmann approximations for the mathematical description of the kinetics of industrial processes are described.

A new approach to modeling of industrial processes with unknown mechanism is presented on the base of formulated axiom and theorem. The axiom „Mathematical structure of real process does not depend on the measuring system“ is used for the formulation of the theorem “Mathematical structure of the quantitative description of real systems is possible to be presented as power functions complex”.

An algorithm, for the parameters identification in the power functions complex model, permits to modeling and simulation of industrial processes.

ACKNOWLEDGMENTS

This work is supported by Project of Fundamental Scientific Research 19-58-18004, conducted by RFBR and the National Science Fund of Bulgaria under contract No KP 06 RUSIA-3 from 27 Sep. 2019, “Modeling, simulation and experimental investigations of the interphase mass transfer and separation in distillation, absorption, adsorption and catalytic processes in industrial column apparatuses”.

References

1. Boyadjiev, Chr., Theoretical Chemical Engineering. Modeling and simulation, *Springer-Verlag, Berlin Heidelberg*, 2010.
2. Keizer, J., Statistical Thermodynamics of Nonequilibrium Processes, *Springer-Verlag, New York*, 1987.
3. Boyadjiev, Chr., Reaction kinetics in chemical engineering, *Bulgarian Chemical Communications*, 2018, vol. 50(Special Issue-K), pp. 112-119.
4. Boyadjiev, Chr., Some Thoughts on Logic and Intuition in Science and Chemical Engineering, *Open Access Library Journal*, 2014, vol. 1, no. 6, pp. 1-5.
5. Гухман, А. А., Введение в теорию подобия, *Изд. „Высшая школа“, Москва*, 1973, (Gukhman, A. A., Introduction to the theory of similarity, *Ed. „Higher School“, Moscow*, 1973).

Multicriterial optimization strategies for electron beam grafting of corn starch

Lilyana Koleva[1*], Zlatina Petrova[1], Elena Koleva[1,2**], Mirela Braşoveanu[3], Monica R. Nemţanu[3], Georgi Kolev[1]
University of Chemical Technology and Metallurgy, Bulgaria[1]
Institute of Electronics, Bulgarian Academy of Sciences, Bulgaria[2]
National Institute for Lasers, Plasma and Radiation Physics, Electron Accelerators Laboratory, Romania[3]
sura@uctm.edu[*], eligeorg@uctm.edu[**]

Abstract: *Grafting is the most effective way of modifying and regulating the properties of natural polysaccharides for the production of highly efficient graft copolymers, which have applications as flocculating agents for the treatment of different wastewaters. An experimental investigation connected with the modification of starch by grafting acrylamide with the application of electron beam irradiation is performed. In this paper the implementation of different multi-criteria optimization strategies, solving the problem with the choice between several compromise Pareto-optimal solutions are presented and compared for the process of electron beam grafting of corn starch. The compromise Pareto-optimal solutions are obtained by implementation of genetic algorithm and a set of requirements for the desired reference direction (minimum or maximum) and the constraints of the investigated quality characteristics and their variances under production conditions, which ensure the fulfilment of several goals – economic efficiency, assurance of low toxicity and high copolymer efficiency in flocculation process.*

Keywords*: GRAFT COPOLYMERIZATION, ELECTRON BEAM IRRADIATION, WATER-SOLUBLE COPOLYMERS, STARCH, ACRYLAMIDE, FLOCCULATION PROPERTIES, MULTI-CRITERIA OPTIMIZATION, DECISION MAKING*

1. Introduction

Electron beam (EB) grafting is a process that is able to modify the polymer substrates by implementing radiation-induced graft copolymerization in order to yield water-soluble copolymers for flocculation processes [1-3]. It is widely used to develop a wide variety of ion exchangers, polymer-ligand exchangers, chelating copolymers, hydrogels, affinity graft copolymers and polymer electrolytes, having various applications in water treatment, chemical industry, biotechnology, biomedicine, etc. [4].

Robust or not sensitive to noises and errors engineering approach can be implemented when analyzing experiments during which the variance is non-homogeneous over the factor (process parameters') space and when the noise factors cannot be identified nor an experiment to study them can be conducted [5, 6]. The observations in this case are called heteroscedastic (variance varies with the factor levels). This is the situation, when the analyzed data are obtained under production conditions. In order to estimate the variances of the quality characteristics there are several approaches. In the current investigation the models for the mean values and the variances of the quality characteristics of the product, are estimated by performing repeated observations. Multicriterial parameter optimization in terms of obtaining repeatability of the product parameters and quality improvement at the same time is performed by minimization of variations of the quality characteristics and fulfilling the technological requirements for these characteristics in production conditions simultaneously.

In this paper the implementation of different multi-criteria optimization strategies, solving the problem with the choice between several compromise Pareto-optimal solutions are presented and compared for the process of electron beam grafting of corn starch. The compromise Pareto-optimal solutions are obtained by implementation of genetic algorithm and a set of requirements for the desired reference goals (minimum or maximum) and the constraints of the investigated quality characteristics and their variances under production conditions, which ensure the fulfilment of several goals – economic efficiency, assurance of low toxicity and high copolymer efficiency in flocculation process.

2. Experimental conditions

Experiments for the modification of starch by grafting acrylamide using electron beam irradiation were performed in order to synthesize water-soluble copolymers having flocculation abilities. The synthesis of graft copolymers was performed by two steps: (1) preparation of solutions containing starch and monomer; (2) irradiation of solutions by electron beam.

Step 1: Starch aqueous solutions were prepared by dissolving corn starch in distilled water. Acrylamide was added to starch aqueous solution with further stirring, resulting in various acrylamide/starch (AMD/St weight ratios) homogenous aqueous solutions.

Step 2: Therefore, homogenous aqueous solutions prepared in previous step were exposed to electron beam irradiation. The irradiations were carried out at ambient temperature and pressure by using linear electron accelerators of mean energy of 6.23 MeV with different irradiation doses and dose rates.

The synthesized graft copolymers were characterized by residual monomer concentration, Mr, %; monomer conversion coefficient, Conv., % and intrinsic viscosity, η, dL/g. The variation regions of the process parameters were: for EB irradiation dose (z_1) - 0.65 ÷ 5.50 kGy, the dose rate (z_2) – 0.41 ÷ 1.50 kGy/min and the AMD/St weight ratio (z_3) – 2 ÷ 11.

The dependencies of the mean values and the variances of the product quality characteristics: residual monomer concentration - y_1 (%), monomer conversion coefficient - y_2 (%) and apparent viscosity - y_3 (mPa·s) on the variation of the process parameters: electron beam irradiation dose, electron beam irradiation dose rate and AMD/St weight ratio are estimated.

The estimated mean value $\tilde{\bar{y}}_{ui}$ and $\tilde{s}^2_{ui}$ variance can be considered as two responses at the design points, and ordinary least squares method can be used to fit the models of the mean value and the variance for the quality characteristic [6, 7]:

$$(1) \qquad \tilde{\bar{y}}(\vec{x}) = \sum_{i=1}^{k_y} \hat{\theta}_{yi} f_{yi}(\vec{x})$$

$$(2) \qquad ln\left(\tilde{s}^2(\vec{x})\right) = \sum_{i=1}^{k_\sigma} \hat{\theta}_{\sigma i} f_{\sigma i}(\vec{x}),$$

where $\hat{\theta}_{yi}$ and $\hat{\theta}_{\sigma i}$ are estimates of the regression coefficients, and f_{yi} and $f_{\sigma i}$ are known functions of the process parameters x_i.

The obtained models for the mean values $\tilde{\bar{y}}_j$ and the variance $\tilde{s}_j^2$ for each of the considered $j = 1, 2, ..., m$ quality characteristics are presented and discussed in [4].

3. Multicriterial optimization

In the case of EB induced grafting of corn starch multi-criteria optimization unifying requirements for economic efficiency, assurance of low toxicity and high copolymer efficiency in flocculation process, as well as the repeatability of the obtained results is performed.

The set of defined technological requirements is the following:

- residual monomer concentration: $\tilde{\bar{y}}_1 < 5\% \rightarrow$ assurance of low toxicity;
- monomer conversion coefficient: $\tilde{\bar{y}}_2 > 90\% \rightarrow$ economic efficiency;

- apparent viscosity: $\tilde{\bar{y}}_3$ > 3 mPa·s → copolymer efficiency in flocculation processes.

For the satisfaction of all pre-defined requirements simultaneously the optimization task is set as follows:

$\tilde{\bar{y}}_1$ → minimum, $\tilde{\bar{y}}_1$ < 5%;
$\tilde{\bar{y}}_2$ → maximum, $\tilde{\bar{y}}_2$ > 90%;
$\tilde{\bar{y}}_3$ → maximum, $\tilde{\bar{y}}_3$ > 3 mPa·s;
$\tilde{\sigma}_1^2$ → maximum;
$\tilde{\sigma}_2^2$ → maximum;
$\tilde{\sigma}_3^2$ → maximum.

The implemented for solving the multicriterial optimization task models for the mean values $\tilde{\bar{y}}_j$ and the variance $\tilde{s}_j^2$ for each of the considered *j = 1, 2, ..., m* quality characteristics are presented in [4].

Pareto-optimal compromise solutions are obtained (50 solutions) by applying genetic algorithm and the statistical software QstatLab [8]. Each solution makes some compromise toward some or all quality criteria to a certain extend at the same time. If we compare randomly chosen two Pareto-optimal solutions some of the quality characteristics will have better values, but at least one will be worse. In order to choose one solution from all we need additional analysis. This choice can be done by considering additional criteria (not included in the optimization task), by evaluation based on expert opinion or by definition of an overall function like loss function, desirability function, etc.

In the present work, methods based on reference point strategies optimization are implemented for solving this task. They are compered by estimation of the overall relative error for all best solutions that are obtained.

Optimistic strategy

The *optimistic strategy* is based on the method of the function of losses. This optimization approach is called "optimistic" because the best possible values q_j^{Opt} (*j* = 1, 2, 3, …, *m*) are assigned to the reference (uncompromised) values of the quality characteristic $q_i(x)$. The reference values depend on the required minimum or maximum value for each of the quality characteristics. They are determined from the obtained Pareto-optimal solutions or in this case the differences between the best values and the optimistic reference values are minimized. The generalized function of losses $F^{Opt}(x)$ that has to be minimized is [9]:

$$F^{Opt}(x) = \frac{1}{m}\sum_{j=1}^{m}\left(\frac{q_j^{Opt} - q_j(x)}{\Delta_j}\right)^2, \quad (4)$$

$$\Delta_j = q_{max,j} - q_{min,j}, \quad (5)$$

where $q_j(x)$ is the value for the *j-th* quality characteristic obtained at a given Pareto-optimal solution, $q_{max,j}$ and $q_{min,j}$ are the maximal and minimal values of each characteristic from all obtained 50 Pareto-optimal solutions and are presented in Table 1, together with calculated value for Δ_j. Each reference value q_j^{Opt} is obtained usually for different set of optimal process parameters z_i and cannot be obtained simultaneously.

Table 1: *Goals, reference values and the maximal and minimal characteristic values $q_i(x)$.*

Param.	$\tilde{\bar{y}}_1$ %	$\tilde{\sigma}_1^2$	$\tilde{\bar{y}}_2$ %	$\tilde{\sigma}_2^2$	$\tilde{\bar{y}}_3$ mPa·s	$\tilde{\sigma}_3^2$
Goal	min ↓	min ↓	max ↑	min ↓	max ↑	min ↓
q_j^{Opt}	0.003	0.008	98.689	0.163	5.564	0.163
q_j^{Pes}	4.996	0.136	90.874	3.602	3.359	0.617
$q_{j,max}$	4.996	0.136	98.689	3.602	5.534	0.617
$q_{j,min}$	0.003	0.008	90.874	0.163	3.359	0.163
Δ_j	4.996	0.128	7.815	3.439	2.175	0.454

The best ten optimal solutions obtained by implementation of the Optimistic method are presented in Table 2. They have smallest values of the function of losses $F^{Opt}(x)$ from the arranged in ascending order results from all obtained 50 Pareto-optimal solutions (their numbers are kept in the table). It can be seen that the best result, obtained for $F^{Opt}(x)$ = 0.128 is obtained for Pareto-optimal solution № 10, as well as the optimal values of the process parameters (z_i) at which it can be obtained in production conditions.

Table 2: *Optimal solution by Optimistic strategy.*

№	F^{Opt}	z_1	z_2	z_3	$\tilde{\bar{y}}_1$	$\tilde{\sigma}_1^2$	$\tilde{\bar{y}}_2$	$\tilde{\sigma}_1^2$	$\tilde{\bar{y}}_3$	$\tilde{\sigma}_1^2$
10	**0.128**	**4.7**	**0.6**	**3.9**	**1.4**	**0.06**	**98.2**	**0.95**	**4.09**	**0.19**
9	0.129	4.8	0.6	3.8	1.0	0.07	96.6	0.82	4.39	0.19
43	0.130	4.7	0.6	4.0	1.3	0.06	98.3	0.95	4.01	0.18
28	0.144	5.1	1.1	2.0	3.9	0.02	97.1	0.19	4.99	0.34
22	0.149	5.1	1.1	2.3	3.6	0.03	95.4	0.23	4.78	0.27
39	0.153	4.9	0.6	3.9	1.9	0.07	95.6	0.90	4.22	0.18
2	0.154	5.0	1.0	2.7	3.3	0.02	94.7	0.28	4.61	0.22
30	0.156	5.0	1.1	3.4	3.4	0.02	94.9	0.24	4.61	0.25
6	0.172	4.8	0.6	4.2	1.6	0.06	95.4	1.00	3.95	0.16
18	0.176	5.2	1.1	2.0	4.2	0.03	95.4	0.19	5.15	0.32

Pessimistic strategy

The pessimistic strategy is based on the function of usefulness method. In this strategy the worst possible (among the obtained Pareto-optimal solutions) or the "pessimistic" values q_j^{Pes} (*j = 1, 2, 3, …, m*) are assigned as reference values of the quality characteristic $q_i(x)$, again depending on the required minimum or maximum value for each quality characteristic from Pareto-optimal solutions. The function $F^{Pes}(x)$ that has to be maximized is [9]:

$$F^{Pes}(x) = \frac{1}{m}\sum_{j=1}^{m}\left(\frac{q_j(x) - q_j^{Pes}}{\Delta_j}\right)^2 \quad (6)$$

The best ten optimal solutions obtained by implementation of the Pessimistic strategy are presented in Table 3. They have largest values of the function of usefulness $F^{Pes}(x)$ from the arranged in descending order results from all obtained 50 Pareto-optimal solutions (their numbers are kept in the table).

Table 3: *Optimal solution by Pessimistic strategy.*

№	F^{Pes}	z_1	z_2	z_3	$\tilde{\bar{y}}_1$	$\tilde{\sigma}_1^2$	$\tilde{\bar{y}}_2$	$\tilde{\sigma}_1^2$	$\tilde{\bar{y}}_3$	$\tilde{\sigma}_1^2$
43	**0.571**	**4.7**	**0.6**	**4.0**	**1.3**	**0.06**	**98.3**	**0.95**	**4.01**	**0.18**
28	0.560	5.1	1.1	2.0	3.9	0.02	97.1	0.19	4.99	0.34
10	0.559	4.7	0.6	3.9	1.4	0.06	98.2	0.95	4.09	0.18
18	0.526	5.2	1.1	2.0	4.2	0.03	95.4	0.19	5.15	0.32
22	0.522	5.1	1.1	2.3	3.6	0.03	95.4	0.23	4.78	0.27
42	0.522	4.9	0.5	3.2	2.6	0.12	98.0	0.68	5.29	0.28
23	0.518	5.3	1.0	2.4	4.7	0.05	91.2	0.21	5.47	0.24
2	0.515	5.0	1.0	2.7	3.3	0.02	94.7	0.28	4.61	0.22
1	0.514	5.4	1.1	2.0	4.9	0.03	91.4	0.16	5.53	0.32
49	0. 514	5.2	1.0	2.4	4.5	0.04	92.5	0.21	5.36	0.25

Bracketing approach for multi-criteria optimization

The bracketing multi-criteria optimization strategy combines the optimistic and pessimistic approaches. Here the optimal compromise solution is searched by simultaneously minimizing the under-achievement to the best values (reference values) q_j^{Opt} and maximizing the over-achievement over the required (worst) values q_j^{Pes} [9].

The optimization function that has to be maximized in this case is:

$$F^{Br}(x) = \frac{1}{m}\sum_{j=1}^{m}\left(\frac{q_j(x) - q_j^{Pes}}{\Delta_j}\right)^2 - \frac{1}{m}\sum_{j=1}^{m}\left(\frac{q_j^{Opt} - q_j(x)}{\Delta_j}\right)^2 \quad (7)$$

The best ten optimal solutions obtained by implementation of the Bracketing strategy are presented in Table 4. They have largest values of the function of usefulness $F^{Br}(x)$ from the arranged in descending order results from all obtained 50 Pareto-optimal solutions (their numbers are kept in the table).

It can be seen, that the best result in this case coincides with the best result obtained when the Pessimistic strategy is applied (Pareto-optimal solution №43).

Table 4: *Optimal solution by Bracketing approach.*

№	F^{Br}	z_1	z_2	z_3	$\tilde{y}_1$	σ_1^2	$\tilde{y}_2$	σ_2^2	$\tilde{y}_3$	σ_3^2
43	**2.777**	**4.7**	**0.6**	**4.0**	**1.3**	**0.06**	**98.3**	**0.95**	**4.01**	**0.18**
10	2.750	4.7	0.6	3.9	1.4	0.06	98.2	0.95	4.09	0.18
42	2.647	4.9	0.5	3.2	2.6	0.12	98.0	0.68	5.29	0.28
9	2.361	4.8	0.6	3.8	2.0	0.07	96.6	0.82	4.39	0.19
28	2.359	5.1	1.1	2.0	3.9	0.02	97.1	0.19	4.99	0.34
37	2.291	5.0	0.7	3.2	3.1	0.10	95.9	0.54	5.31	0.25
22	2.099	5.1	1.1	2.3	3.6	0.03	95.4	0.23	4.78	0.27
26	2.069	5.1	0.6	3.2	3.2	0.11	95.4	0.57	5.42	0.26
2	2.049	5.0	1.0	2.7	3.3	0.02	94.7	0.28	4.61	0.22
14	2.026	4.7	0.5	4.6	0.6	0.08	98.0	1.74	3.73	0.19

In order to compare the implemented optimization strategies: *Optimistic and Pessimistic/Bracketing approaches*, the absolute errors are calculated for the best chosen compromise solutions by:

$$\delta_{aj} = \left| q_{j,opt}(x) - q_j{}^*(x) \right|$$

where $q_j{}^*(x)$ is the best value from all Pareto-optimal solutions for the *j-th* quality characteristic, coinciding with the reference point of the optimistic approach. The relative error in this case can be calculated by:

$$\delta_{rj} = \frac{\delta_{aj}}{\Delta_j} * 100\%$$

The calculated results are presented in Table 5.

Table 5: *Comparison of implemented optimization strategies.*

№	$\tilde{y}_1$	σ_1^2	$\tilde{y}_2$	σ_2^2	$\tilde{y}_3$	σ_3^2
q_j^*	0.003	0.008	98.689	0.163	5.564	0.163
Δ_j	4.996	0.128	7.815	3.439	2.175	0.454
$\boldsymbol{q_{j,opt}}$, *Opt*	1.4	**0.06**	98.2	**0.95**	**4.09**	0.19
$\boldsymbol{\delta_{aj}}$	1.397	0.052	0.489	0.787	1.474	0.027
$\boldsymbol{\delta_{rj}}$**,%**	27.96	40.63	6.26	22.88	67.77	5.95
$\boldsymbol{q_{j,opt}}$, *Pes/Br*	**1.3**	**0.06**	**98.3**	**0.95**	4.01	**0.18**
$\boldsymbol{\delta_{aj}}$	1.297	0.052	0.389	0.787	1.554	0.017
$\boldsymbol{\delta_{rj}}$**,%**	25.96	40.63	4.98	22.88	71.45	3.74

From Table 5 can be seen that the implemented strategies give very close results. The only quality parameter, which is a little better for the solution, given by the Optimistic approach, is the result for the apparent viscosity $\tilde{y}_3$, responsible for copolymer efficiency in flocculation processes. All the other criteria values are better or equal for the case of implementation of the pessimistic or bracketing strategies.

4. Conclusions

In this paper, three multicriteria optimization approaches were applies and compared, aiming to simultaneously fulfil the technological requirements for economic efficiency, assurance of low toxicity and high copolymer efficiency in flocculation process, as well as the repeatability of the obtained results.

The implementation of multi-criteria optimization strategies, by definition of one overall optimization criterion, solves the problem with the choice between several compromise Pareto-optimal solutions. Optimistic, pessimistic and bracketing multi-criteria optimization strategies are implemented and compared for the process of electron beam grafting of corn starch.

The comparison of obtained best working regimes of the applied multi-criteria optimization strategies give very close results. The biggest compromise is done with the apparent viscosity $\tilde{y}_3$, responsible for copolymer efficiency in flocculation processes, which is around 70% from the region of the optimal values of obtained Pareto-optimal solutions Δ_3.

Acknowledgements

This research was conducted under the contracts: bilateral joint project between the Bulgarian Academy of Sciences and The Romanian Academy, and KP-06-N27/18, funded by the National Fund “Scientific Investigations”.

References

1. G. Craciun, E. Manaila, M. Niculescu, D. Ighigeanu, Polym. Bull. 1299 (2017)
2. M. R. Nemţanu, M. Braşoveanu, Polymer science: research advances, practical applications and educational aspects, ed. A Méndez-Vilas and A. Solano-Martín (Badajoz: Formatex Research Center) 270-277 (2016)
3. M. Braşoveanu, L. St. Koleva, M. R. Nemţanu, E. G. Koleva, T. P. Paneva. J. of Phys.: Conf. Ser., 1089 (2018)
4. L. Koleva, E. Koleva, M. Nemtanu, M. Braşoveanu, Inter. Sci. J. of Sci. Tech. Union of Mech. Eng. "Industry 4.0", **4**, 2, 48-51 (2019)
5. E. Koleva, I. Vuchkov, Vacuum, **77**, 423-428 (2005)
6. I. N. Vuchkov, L. N. Boyadjieva, *Quality improvement with design of experiments* (The Netherlands, Kluwer Academic Publishers, 2001)
7. S. Najafi, A. Salmasnia, R. B. Kazemzadeh, AJBAS, **5**/9, 1566-1577 (2011)
8. QstatLab home page: http://www.qstatlab.co.uk/eng/index.html
9. S. Stoyanov, Bioautomation, **13**(2), 1-18 (2009)

Implementation of simulation tools in optimization of traffic flows – case study City of Zagreb

Nikola Kožul[1,*], Luka Novačko[2]
Ernst&Young Ltd., Zagreb, Croatia[1]
Faculty of Transport and Traffic Sciences, Zagreb, Croatia[2]
luka.novacko@fpz.unizg.hr

Abstract: *Urbanization and population growth in cities around the world have increased the degree of motorization, which ultimately results in congestion of the transport network within these cities. Traffic simulation tools are essential for the optimization and evaluation of variant solutions in road traffic. By analysing traffic parameters from simulation results it can be decided which variant solution is optimal without high financial inputs. In this paper, the most important simulation tools are explained. As a case study, one district in the City of Zagreb was chosen to present possibilities of simulation tools and their implementation in the evaluation of traffic solutions.*
Keywords*: TRAFFIC MODELLING, SIMULATION TOOLS, CITY OF ZAGREB, OPTIMIZATION*

1. Introduction

The organization of traffic flows is an essential element in the successful operation of the transport system in a designated area. The main goal of traffic optimization is to minimize the cost of traffic flow which is achieved by minimization of crossings on critical intersections in favor of reducing lost time. If organization of traffic flows is not properly optimized, it is possible to create traffic congestions on specific locations what finally affects on complete traffic system [1].

Transport modeling is an integral part of traffic engineering that is used in phases of planning and design. Simulation models are developed to test new solutions and how those new solutions or changes in traffic organization will affect the flow of traffic in the analyzed area. A model is a simplified representation of a part of the real world/system, which focuses on the individual and certain elements considered important from a point of view. Transport models are abstract models based on mathematical formulas and laws. The main elements in the development of transport model simulation are the relationship between traffic demand and traffic supply, where traffic demand is the distribution of activities in space, while traffic supply is defined as the capacity of transport network elements (road, terminals, hubs).

The demand for transport services is highly qualitative and differentiated. There is a whole range of specific demands for transport which are differentiated by time of day, day of the week, journey purpose, type of cargo, the importance of speed and frequency, and so on. A good deal of the demand for transport is concentrated on a few hours of a day, particularly in urban areas where most of the congestion takes place during specific peak periods. Transport supply is service; therefore, it is not possible to stock it and transport service must be consumed when and where it is produced. For this reason, it is very important to estimate demand with as much accuracy as possible to save resources by tailoring the supply of transport services to it [2].

In this paper an overview of the most important simulation tolls will be presented and in the other part of paper an example of implementation of simulation tool VISSIM in the City of Zagreb will be shown.

2. Overview of simulation tools

Traffic simulation is an indispensable instrument for transport planners and traffic engineers. In this chapter some of the most used traffic simulation software will be described.

Modern traffic simulation tools are based on different principles and have two main origins: industrial and academic ones. Industrial simulators (e.g., Vissim, Aimsun), developed for commercial purposes, are generally easier to use and offer user assistance. However, they are less extensible and offer less flexibility and limit the user to predefined cases. The second group of simulators comes from research labs. Developed as part of research work, these solutions are usually less complete and not easy to use for an uninitiated user [3].

Simulation tools offer different levels of traffic modeling usually classified into three following groups: macroscopic, microscopic, and mesoscopic. In macroscopic models, vehicle flow is assimilated to the runoff of a fluid in a pipe and modeled through the equations of fluid mechanics. In contrast, in microscopic and mesoscopic approaches, each actor of the traffic is respectively considered individually and in small homogeneous groups [3].

VISSIM is a microscopic, behavior-based multi-purpose traffic simulation to analyze and optimize traffic flows. It offers a wide variety of urban and highway applications, integrating public and private transportation. Complex traffic conditions are visualized in high level of detail supported by realistic traffic models. VISSIM is a commercial software tool with about 7000 licenses distributed worldwide in the last 15 years. About one-third of the users are within consultancies and industry, one-third within public agencies, and the remaining third is applied at academic institutions for teaching and research. VISSIM is a microscopic, discrete traffic simulation system modeling motorway traffic as well as urban traffic operations. Based on several mathematical models, the position of each vehicle is recalculated every 0.1–1 s. The system can be used to investigate private and public transport as well as in particular pedestrian movements [4].

S-Paramics is used on a wide variety of transport-modelling projects. The strength of S-Paramics is in its ability to apply microsimulation to large area models. The ‘micro’ in microsimulation reflects the level at which the interactions between vehicles are modelled, not a limit to the size of the geographical area in a model. Large models may cover tens of squares of kilometres with hundreds of zones and hundreds of kilometres of road network [4].

The Aimsun transport modelling software is a long-term research programme at the University of Catalonia (UPC), Spain. the software now includes macroscopic, mesoscopic and microscopic models. Expanding in response to practitioners’ requirements, Aimsun has come to encompass a collection of dynamic modelling tools. Specifically, these include mesoscopic and microscopic simulators and dynamic traffic assignment models based on either user equilibrium or stochastic route choice [4]e.

“Simulation of Urban MObility”, or “SUMO” for short, is a microscopic road traffic simulation. The work on SUMO’s design began in the year 2000, with the first implementation being started in the year 2001. SUMO is available as “open source” under the GNU General Public License, both as source code and in compiled, executable form for multiple Windows and Linux platforms. The reason for building an open-source traffic simulation was that while working on traffic simulations within the academic field, it was noted that many different, small simulations were developed as tools within diploma or doctoral theses, in order to evaluate the objective that was the thesis’ real topic [4].

3. Implementation of simulation tools – City of Zagreb example

Transport network capacity is one of the most important attributes while analyzing transport networks. Capacity defines maximum number of vehicles crossing a section of road per unit of time at any selected period. City of Zagreb Master Plan defines current traffic capacities on road network in City of Zagreb area and it is used as a starting point in analyzing transport network in that area. Master Plan data defines the capacity of all types of roads. City avenues have a capacity from 1.000 up to 3.000 vehicles in one way per hour, while other road types have a capacity of under 1.000 vehicles in one way per hour [5].

Same as capacity, the volume of traffic is another important attribute used to analyze traffic congestions on a traffic network. Traffic volume presents the number of vehicles crossing a section of road per unit time at any selected period. The volume/capacity (V/C) ratio is one of the most important elements of transport that describes the state of the transport network. The result given by V/C ratio expresses road congestion, namely, usage of road capacity on the analyzed road. It is also often used as a precautionary measure to detect roads that are near to congestion level. Congestion arises when demand levels approach the capacity of a facility and the time required to use it (travel through it) increases well above the average. [2] Congestion level is considered every V/C/ ratio over 0,75 or 75 %. If the ratio is over 75 % it is necessary to present optimal solutions to reduce congestions. If the ratio value is over 1,00 or 100 %, it is considered that analyzed network demand is higher than supply.

During the development of the Master Plan of the City of Zagreb, a transport model of the City of Zagreb and surrounding counties were created in the simulation tool PTV Visum, which shows the current state of roads in the analyzed area as seen in **Fig 1**.

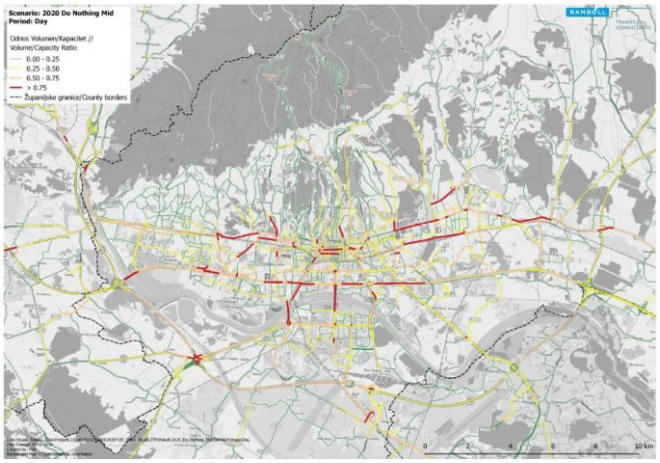


Fig 1. *V/C ratio in City of Zagreb area*

In this paper, one city district in the City of Zagreb is analyzed to evaluate the effects of the proposed traffic optimization solutions using simulation tools. The analyzed city district is located in the northern part of the city and is characterized by geographical and traffic limitations and traffic congestions during weekends due to increased recreational and social activities in the area.

In order to check the relationship between traffic supply and demand and to check the possibility of congestion, macro and microsimulation models were developed as a part of the proposed solution. The macrosimulation model developed in PTV Visum will be used to evaluate new traffic solutions for the construction of a new road to relieve the existing ones and increase the level of traffic safety in the area. The macrosimulation model aims to show the current situation on the transport network and to compare it to the future situation after the implementation of a new road. The microsimulation tool, PTV Vissim, will be used to analyze the reconstruction of the busiest intersection in the whole district and to determine the movement of traffic on the reconstructed intersection.

As previously stated, the district is characterized by congestions during weekends due to large recreational activities that are going to additionally increase in the future with the introduction of a new cable car in the analyzed area. The new cable car will contain an underground garage and outside parking lot with a capacity of about 330 parking places and additional problems in form of traffic congestion are expected in the analyzed area.

The proposal of traffic optimization of the analyzed city district is reflected in the reconstruction of the busiest intersection and the construction of a new transversal road for additional connection of the neighborhood with the city center.

The simulation of the newly proposed intersection reconstruction was performed in the PTV Vissim simulation tool by creating a model of reconstructed intersection. The creation of the model required the creation of modeled intersection from zero.

As a first step in creating a transport model, traffic counting has been carried out. Traffic counting was performed in one hour period during afternoon peak hour with a goal to receive traffic data during the most congested period of the day. Due to the implementation of a new road in the intersection, traffic count was also conducted on the following intersection with the goal of gathering additional data on traffic distribution.

After traffic counting was carried out, the creation of a transport model in the simulation tool has been started. Firstly, the link and connectors were created that are the foundation of every microsimulation model. Links, that are stand-alone objects, represent roads on the network, while connectors, which must be attached to the previously created link, represent turns on the network. The microsimulation model was created with 55 links and connectors that represent the transport network in the analyzed area.

After the implementation of roads, the next steps were to determine desired speeds, reduced speed on connectors, conflict areas, and priority rules on the analyzed intersection. Data gathered during traffic counting is implemented as vehicle inputs and static vehicle routes attributes. Those attributes describe the number of vehicles passing through the intersection and the distribution of vehicles on it. After implementation of all needed attributes, transport model creation was complete, and the model was simulated as seen in **Fig 2**.



Fig 2. *Simulation process of the developed microsimulation model in PTV Vissim*

After the simulation of the transport model, evaluation data was calculated. Evaluation data were collected to analyze traffic elements on the intersection. Analyzed data consisted of the average speed of vehicles in the intersection, maximum queue lengths on the links, lost time while waiting in the intersection, and level of service for each intersection approach. Data for each of the above-named data are seen in Table 1

.

Table 1: *Data collection measurements from the developed model*

Intersection approach	Average speed [km/h]	Maximum queue length [m]	Lost time [sec]	Level of service
1 – west	46,56	10,37	2,92	LOS A
2 – south	44,87	0,00	3,18	LOS A
3 – east	26,61	54,70	16,33	LOS C
4 – north	27,02	11,55	3,74	LOS B

Unlike evaluation of results within the microsimulation model, within the macrosimulation model, the data of congestion of the complete traffic network is analyzed in the monitored area.

As the most common parameter used to evaluate the transport network when monitoring private transport within the macrosimulation model is certainly the traffic volume that passes through a certain section of traffic in a certain time interval. Within created macrosimulation, the traffic volume was presented for a period of one day.

The development of the macrosimulation model was conducted within the PTV Visum simulation tool, which is used to show the entire traffic network in the analyzed area. Input data of the amount of traffic entering the area of the transport network were obtained by field research, i.e. by counting traffic on characteristic locations. Traffic counting data were obtained in a period of one hour and was recalculated to AADT (annual average daily traffic) to implement it to the model.

Macrosimulation models are built from a few network elements that recreate the analyzed area. The first element is nodes that represent intersections on roads, the second element is links that represent transport network, and the third element are zones that represent areas from where and where to trips happen. Created macrosimulation model contains 145 nodes, 314 links, and 28 zones that represent the analyzed area.

Created macrosimulation model (**Fig 3.**) was used to test the construction of a new road that should relieve the existing transport network and ensure an increased level of safety on insecure intersections.

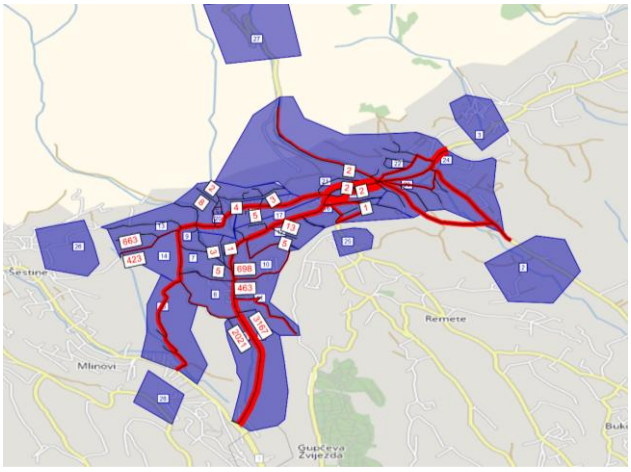


Fig 3. *Macrosimulation model of the district in City of Zagreb created within PTV Visum*

After the implementation of the traffic network simulation with implemented solution, a major change in the distribution of traffic in the analyzed area was visible. Newley implemented transversal road took over around 50 % of existing traffic, relieving existing busiest road in the area by 50 %. Such relief in traffic congestion can ensure a high level of service and a high level of safety for all users.

4. Conclusion

With the increase in population on the outskirts of the city, roads built in the past find it much harder to handle the traffic currently passing through such an area. Due to spatial possibilities, peripheral settlements in the analyzed area of the City of Zagreb have very narrow roads which make it difficult for two-way traffic. In such a state is the traffic network in the area of the analyzed city district. As part of this paper, an analysis of the current state of road transport infrastructure and the transport system in the analyzed area was carried out, and based on the obtained results, conceptual solutions were given for the purpose of optimizing and improving the transport system.

By developing simulation models and evaluating the results of simulations, conclusions were obtained that the implemented solutions are suitable and that they fulfill the purpose of implementation, ie to optimize and improve the traffic system in the entire area of the analyzed district in the City of Zagreb.

5. References

1. M. Šoštarić, A. Ščukanec, *Authorized lectures from the course Traffic Technology Designing*, Faculty of Transport and Traffic Sciences, (2020)
2. J. Ortuzar, L. Willumsen, *Modelling Transport*, Wiley, Hoboken, (2011)
3. A. O. Diallo, G. Lozenguez, A. Doniec, R. Mandiau, *Comparative Evaluation of Road Traffic Simulators based on Modeler's Specifications: An Application to Intermodal Mobility Behaviors*. Proceedings of the 13th International Conference on Agents and Artificial Intelligence - ICAART 2021, (2021)
4. J. Barceló, *Fundamentals of Traffic Simulation*, Springer, (2010)
5. *Master Plan of the transport system of the City of Zagreb, Zagreb county and Krapina-zagorje county*, City of Zagreb, (2017)

Numerical modeling of impact interaction between an active element and a deformable barrier

Krumov Angel., Simeonova Antoaneta
Institute of Metal Science, Equipment and Technology with Hydroaerodynamic Center at Bulgarian Academy of Sciences,
67 Shipchenski Prohod Street, 1574 Sofia, Bulgaria[1]

***Abstract**: A methodology for calculating the impact interaction between an active element and a deformable barrier is developed on the basis of approximated analytical results. As an active element is considered a hemisphere smoothly shaped into a cylinder. Results from calculations using the proposed methodology are applied. The examples presented here are two extreme cases of interaction that differ from each other by the initial angle of contact of the active element with the barrier.*

***Keywords**: active elements, high-energy formation*

1. Introduction

One of the important aspects of the mathematical modeling of high-speed penetration problems is the need to obtain equations most fully and adequately defining the behavior of the contact materials in test conditions [1, 2, 3, 4]. In order to describe as adequately as possible the physical processes that accompany impact and penetration, such mathematical models must be workable and applicable in practice.

2. Numerical modeling of the impact interaction between an active element and a deformable barrier

Based on approximate analytical results, a methodology for calculating the impact interaction between an active element and a deformable barrier has been created.

To begin with, several time intervals need to be set. Let the location, velocity and acceleration of any point randomly selected on the surface of the active element at the initial moment $t = t_0$, as well as the geometry of the barrier at time $t = t + \Delta t$, be known.

Contact points are those on the surface of the active element for which the following conditions are met:

- the point is in contact at any time t in the interval $t_0 \le t \le t_0 + \Delta t$;
- the projection of the velocity of a point on the surface of the active element on its external normal is positive.

Since the active element is rigid at the point of contact, the curvature of the barrier surface coincides with the curvature of the surface of the active element.

Stage 1:

I. Determination of the contact surface pressure, depending on the values of the radii of the main curves at any point on the contact surface - $R_1$and R_2, using formulas (1) and (2):

$$p_A(t_0) \to R_1 = R_2 = R;$$

$$p_A(t_0) = 2.\sqrt{6}.\tau.ln\left(1+\frac{h}{R}\right) + \rho\left[2.V_0^2(t_0) + R.\frac{dV_0}{dt}\right].\frac{h}{R+h} - \rho V_0^2(t_0).\frac{h(h+2R).(h^2+2.R.h+2.R^2)}{2(R+h)}. \quad (1)$$

$$p_A(t_0) \to R_1 \neq R_2$$

$$p_A(t_0) = 2.\sqrt{2\tau}\left\{\sqrt{3}.ln\frac{2.\sqrt{3}.K+3(R_1+h)}{2.\sqrt{3}\sqrt{R_1^2+R_1.R_2+R_2^2}+3.(R_1+R_2)} + (R_1-R_2)\right\} ln\frac{[2K-R_1-h-2(R_2+h)](R_2+h)}{[2K+2(R_1+h)+R_2+h](R_1+h)} + (R_1-R_2)$$

$$ln\frac{R_1.\left(2\sqrt{R_1^2+R_1.R_2+R_2^2}+2.R_1+R_2\right)}{R_2.\left(2\sqrt{R_1^2+R_1.R_2+R_2^2}-R_1-2R_2\right)} + \rho.\left[(R_1+R_2)V_0^2(t_0)+R_1.R_2.\frac{dV_0}{dt}\right].\frac{1}{R_1-R_2}.ln\frac{R_1(R_2+h)}{R_2(R_1+h)} - \rho V_0^2(t_0)\frac{h(h+R_1+R_2)[h^2+(R_1+R_2)h+2R_1.R_2]}{2(R_1+h)^2(R_2+h)^2}. \quad (2)$$

II. From the obtained pressure distribution we find the new acceleration of the active element and its position at time $t + \Delta t$.

Stage 2:

I. Determination of the geometry of the barrier using formulas (3) and (4):

$$u(0,t) = V(t) = \int_{t_0}^{t} V_0(\tau)d\tau \cong V_0(t_0).\Delta t + \frac{1}{2}.\frac{dV_0}{dt}.\Delta t \quad (3)$$

$$h(t) = h(t_0) - \frac{h(t_0)[h(t_0)+R_1+R_2]}{[R_1+h(t_0)].[R_2+h(t_0)]}.\left[V_0(t_0).\Delta t + \frac{\Delta t^2}{2}.\frac{dV_0}{dt}\right] + \frac{(R_1+R_2).V_0^2(t_0).\Delta t^2}{2.[R_1+h(t_0)].[R_2+h(t_0)]} \quad (4)$$

3. Methodology for calculating the impact interaction between an active element and a deformable barrier

The surface is divided into elementary segments, at the center of which are the calculation points. The geometry of the barrier is described using the spatial position of two surfaces - front and back:

i. For each calculation point of the active element, the distances along the normal to the front surface, as well as the thickness of the barrier are determined.

ii. The calculated point on the front surface of the barrier is shifted in the direction of the normal with the magnitude of the displacement *V (t)* from expression (3).

iii. The calculated point on the back surface is determined using the new barrier thickness from expression (4).

iv. If there is no contact, the calculated points on the surface remain stationary.

v. Determination of the new coordinates of the calculated points on the surface.

vi. Determination of the new position of the active element by means of the forces and moments acting on it.

vii. Determination of the new distance between each point of the active element and the front surface.

viii. Determination of the new thickness of the barrier**.**

When the above actions are concluded, the calculation stage for this step ends, and for each new time step the task restarts from the beginning. The reliability of the calculation is determined by the

division of the active element and the choice of time step. The check for a match with the set trajectory of movement of the active element when reducing the time step serves as a criterion for the stability of the calculation process.

4. Numerical results obtained using the proposed algorithm

1) In case of impact of the active element with the barrier at an angle $\beta = 10$ ° [grad]:

$\beta = 10°[grad],\ t = 2{,}85\,.10^{-4}[s],\ V_c = 1150[m/s],\ \omega = 25[rad/s]$

$\beta = 9°[grad],\ t = 5{,}82\,.10^{-4}[s],\ V_c = 1138[m/s],\ \omega = 83[rad/s]$

$\beta = 8°[grad],\ t = 8{,}78\,.10^{-4}[s],\ V_c = 1129[m/s],\ \omega = 156[rad/s]$

$\beta = 7°[grad],\ t = 13{,}20\,.10^{-4}[s],\ V_c = 1115[m/s],\ \omega = 235[rad/s]$

2) In case of impact of the active element with the barrier at an angle $\beta = 90$ ° [grad]:

$\beta = 90°[grad],\ t = 1{,}37\,.10^{-4}[s],\ V_c = 1136[m/s],\ \omega = -[rad/s]$

$\beta = 90°[grad],\ t = 4{,}50\,.10^{-4}[s],\ V_c = 1042[m/s],\ \omega = -[rad/s]$

4. Conclusion

As the above calculations show, when the active element strikes the barrier at an angle $\beta = 10°$ [grad], the angular velocity ω increases throughout the movement. The speed of movement of the center of gravity *Vc* within the considered time decreases from 1150 to 1115 m/s, and moreover, the component of the speed perpendicular to the plane of the barrier also decreases. This is a case which corresponds to the ricochet phenomenon.

Normal penetration at an angle $\beta = 90$ ° [grad] is of interest as regards the nature of the deformations occurring in the barrier when compared to the penetration of an active element at an acute angle.

The results of this report are aimed at the implementation of Work Package 2 “Intelligent Security Systems” of project BG05M2OP001-1.002-0006 “Construction and development of a Center of Competence “Quantum communication, intelligent security systems and risk management (Quasar)““, which has received funding from the European Regional Development Fund through the Operational Program “Science and Education for Smart Growth” 2014-2020.

References:

1. Malvern in Behavior of Materials Under Dynamic Loading. N. Y., 1995.
2. Simmons J., F. Hauser, J. Dorn.. Mathematical theories of plastic deformation under impulsive loading, 1992.
3. Petkov S., Petkov P., Nikolov G., Tumbarska A.. Mathematical model of the management of high-energy detonation processes through an energy generator (screen). European Journal of Engineering Research and Science, Volume 3, Issue 5, May 2018, EUROPA Publishing, 2018, ISSN:2506-8016, DOI:10.240818/ejers, 65-70
4. Petkov S., Nikolova V.. Modeling of the dynamic properties of the material of the cumulative cladding and the housing in a cumulative unit. V international scientific and technical conference “Engineering. Techologies. Education.Security”, 2017, volume 1, 2017, ISSN:2535-0315 (print), 2535-0323 (online), 94-98

Application of artificial neural networks for prediction of business indicators

Petar Halachev
University of Chemical Technology and Metallurgy – Sofia Bulgaria

Abstract: *This paper examines the applicability of the neural networks in developing predictive models. A predictive model based on artificial neural networks has been proposed and training has been simulated by applying the Long Short-Term Memory Neural Network module and the time series method. Python programming language to simulate the neural network was used. The model uses the stochastic gradient descent and optimizes the mean square error. Business indicators for forecasting the results of the activity and the risk of bankruptcy of a company are forecasted and a comparison of the obtained forecast values with the actual ones is performed in order to assess the accuracy of the forecast of the developed model. As a result, it can be noted that business indicators can be successfully predicted through the Long Short-Term Memory Neural Network and the forecasted values are close to the actual ones.*
Keywords: *FORECASTING, MODEL, LONG SHORT-TERM MEMORY NEURAL NETWORK, BUSINESS INDICATORS, PYTHON*

INTRODUCTION

In modern conditions, one of the most important elements of the management process is the analysis of the indicators reflecting the business activities of the company.

The aim is to establish the patterns and trends in the development of business processes and to assess the direction and degree of influence of the factors that determine them in order to limit the negative and enhance the positive effects. The analysis helps to forecast and design the directions of the future policy of the company by identifying the past trends.

The first approach to analyzing business ratios to predict corporate failure and insolvency was developed by W. Beaver in 1966. Later, various models were developed based on analyzes of groups of companies studied by predefined qualitative characteristics.

The multivariate model for predicting corporate bankruptcy, known as Altman's Z-Score [1], is one of the most widely used models.

Another model, by G. Springate, was developed based on testing of 40 companies, with assets averaging $ 2.5 million. In the process of its creation, out of 19 business coefficients considered representative, only 4 coefficients remain in the final version of the model.

The DuPont model [2] is used for planning, analysis and control of the company's performance and is used in corporate financial management due to the ability to explore the company's potential to generate profit, reinvest it and increase turnover and sales. It is based on the analysis of ratios forming the coefficient Return on Equity (ROE).

Economic value added (EVA) is an analytical model created by the corporate consulting team of B. Stewart and J. Stern and is rapidly gaining popularity among the corporate financial community due to the innovative way of determining the real profitability of the company [3]. The EVA model evaluates the enterprise on the basis of the economic approach and is oriented towards its future and not towards the past. EVA measures the added value created by a particular investment [3, 4].

According to V. Kasarova [5], the application of different models for bankruptcy risk assessment on the same Bulgarian company gives different, in some cases contradictory results, as the models are developed in the conditions of a specific economy in a certain period of time and do not comply with current conditions.

The models do not take into account industry differences, which adversely affects their flexibility and adaptability and leads to excessive optimism or excessive pessimism in some cases. The models can be used as an additional analytical tool and must be appropriately adapted to the specific conjunctural and economic conditions [6, 3].

From the literature sources and the practical activity are known fuzzy models, application of neural networks, econometric analysis and others, to evaluate the business indicators reflecting the activity of the company.

In fuzzy models [7], the analysis and forecasting of financial condition indicators includes 3 stages:

The first stage - "blurring" of the input information, transforming the estimates of traditional indicators into fuzzy values based on expert assessments, modeling and simulation (using Matlab, Fuzzy, Toolbox, etc.).

Second stage - defining the rules according to which the defined fuzzy linguistic variables (inputs) are associated with the output linguistic variable.

Third stage - conversion of the fuzzy estimates obtained at the output of the fuzzy system into exact values.

A common and proven method of blurring is the Geometric Center of Gravity (COG).

Neural networks are used as an additional method for analysis of business indicators. According to A. Chabaan [8], the application of neural networks allows to calculate the risk of failure, decision-making when choosing investment alternatives, assessment of the risk of insolvency of the issuer / borrower [9] and others.

Assessing financial status using artificial intelligence does not replace existing mathematical models, but complements them by allowing the correct assessment of input data, without whose exact values the end result makes no practical sense. According to S. Kabaivanov [9], for example, the process of assessing the risk of insolvency can be realized in two aspects:

On the one hand, obtaining an accurate numerical indicator, individual for each surveyed economic agent (for example, the probability of insolvency for a certain time horizon).

On the other hand, to determine the affiliation of the analyzed object to predefined groups (for example, risk groups with pre-defined boundaries).

FORECASTING THE INDICATORS

Forecasting economic processes and phenomena is a tool for successful and effective business management and has an important role in the management process, as it assists management in making adequate and timely decisions related to the activities of the enterprise.

The report presents a neural network simulation in order to predict the indicators for business analysis. The aim is, on the basis of training of the neural network with indicators from previous periods, to calculate forecast indicators for the next period (in the considered example the data for it are known, and to make comparisons of the actual and forecast values).

After making the forecast, the data from it should be compared with the real data for the respective period and the level of the error from the forecast should be determined. On this basis, conclusions are drawn about the applicability of the model.

Table 1 provides data on the indicators of a real operating enterprise for the period 2011–2019. The indicators from 2019 are taken as a benchmark for comparing the forecast with real data.

Table 1. *Indicators of financial condition*

Indicators	2011	2012	2013	2014	2015	2016	2017	2018	2019
Profitability of income	0.27	0.21	0.18	0.22	0.15	0.16	0.15	0.21	0.11
Return on equity	0.55	0.34	0.24	0.26	0.19	0.18	0.14	0.18	0.08
Return on assets	0.45	0.18	0.15	0.19	0.11	0.12	0.14	0.16	0.07
Revenue efficiency	0.70	0.77	0.80	0.78	0.84	0.82	0.83	0.77	0.88
Cost efficiency	1.42	1.29	1.25	1.27	1.18	1.22	1.20	1.30	1.14
Total liquidity	8.10	5.65	4.44	5.93	2.70	4.89	6.59	10.89	8.17
Quick liquidity	7.30	5.08	4.02	5.45	2.55	4.72	6.29	10.39	7.56
Inventory turnover	17.48	17.93	16.52	35.92	29.23	36.00	35.60	13.00	22.10
Financial autonomy	8.65	1.24	1.73	2.08	1.88	3.14	4.51	7.42	7.37
Financial dependence	0.12	0.81	0.58	0.49	0.53	0.32	0.22	0.13	0.14

The forecasting of the indicators through a neural network is carried out in three stages:

1. Neural network training with known data.
2. Forecasting the indicators.
3. Evaluation of the accuracy of the forecast from the neural network by comparing the predicted with the real values of the indicators.

The method of forecasting time series for training and forecasting [10, 11] has been applied. A separate neural network is created for each of the indicators studied. Each of the neural networks has 3 input parameters and one output.

The information is distributed in a training sample, using the so-called "time window", that covers 3 consecutive years [12], to which the data from the fourth year are compared. For example, for the first indicator in Table 1: the values [0.27; 0.21; 0.18], and at the output [0.22].

The distribution of information is shown in Table 1. The training is performed in 5 stages, and at each stage information is submitted to the neural network in the manner shown in Table 2.

Table 2. *Training sample for the rate of return on income*

Stage	Indicator values (from Table 1)	
	Input	Outcome
1	2011, 2012, 2013	2014
2	2012, 2013, 2014	2015
3	2013, 2014, 2015	2016
4	2014, 2015, 2016	2017
5	2015, 2016, 2017	2018

The neural network is not trained with data for 2019, as the data for it will be used to compare with the data predicted by the model and assess the accuracy of the model

Table 3. *Values of the indicators from the training of the neural network*

Indicators	Value 2019	Forecast 2019	Error (%)
Profitability of income	0.11	0.13	-12.50
Return on equity	0.08	0.10	-4.26
Return on assets	0.07	0.09	-5.26
Revenue efficiency	0.88	0.85	16.67
Cost efficiency	1.14	1.15	-3.57
Total liquidity	8.17	8.03	1.71
Quick liquidity	7.56	7.35	2.68
Inventory turnover	22.10	21.41	3.00
Financial autonomy	7.37	7.02	4.72
Financial dependence	0.14	0.28	-20.29

At the next stage (forecasting by neural network) information about the indicator for 2016, 2017, 2018 is submitted to the model, and the model generates as a result a forecast for the value of the indicator for 2019. Then the forecast value obtained from the model is compared with the real value of the indicator and determine the error of the model.

During the test, 10 neural networks were created, which were trained with samples for each indicator. The data are presented in Table 3.

The Python programming language and the LSTM (Long Short-Term Memory Neural Network model) module to simulate a neural network were used. The neural network architecture is LSTM. The model uses a stochastic gradient version and optimizes the mean square error (Mean Square Error).

The accuracy of the forecast for each indicator is determined as a percentage by the formula:

$$Error\ (\%) = \left(\frac{x_{2019} - x_{forec.}}{x_{\max} - x_{\min}} \right) \times 100 \quad (1)$$

where:

X_{2019} is the value of the indicator for 2019;

$X_{forec.}$ - the forecasted value of the indicator;

X_{max} and X_{min} - the maximum and minimum values of the indicator for the studied period (2011-2019).

When the value of the forecast exceeds the value for 2019, the error is negative, otherwise it is positive.

As a result, the following conclusions can be drawn:

The values of the indicators return on equity, liquidity, financial autonomy and turnover of inventories are predicted by the neural network with high accuracy - the error is within ± 5%.

The indicators turnover of inventories, financial dependence, revenue efficiency, profitability of revenues - the error is high over 20%. In order to reduce this error and increase the accuracy of the prediction in future research, it is appropriate to study a longer time interval so that the neural network can be better trained, as well as to experiment with other structures or neural network models.

BANKRUPTCY RISK ASSESSMENT

Altman's management model was created to predict the viability of industrial exchange companies within 2 years and works with the financial performance of large corporations. As a tool for improving the decision-making process was proposed by E. Tsvetanova, a modified model based on the management model of Altman, which supports the process of determining the viability of small and medium enterprises [13].

The model is adapted to the Bulgarian conditions on the basis of empirical information from Bulgarian enterprises in order to predict whether small and medium enterprises will reach a state of bankruptcy in a period of one to two years with a certain degree of accuracy [14].

Other authors, Avelova, Marchev and team also point to the need to propose weights of Z-score, adapted to the specific economic conditions in which enterprises operate in Bulgaria [15].

Based on a study conducted on Bulgarian companies to adapt Altman's model for assessing the risk of corporate bankruptcy for Bulgarian conditions, E. Tsvetanova [13] proposed a model for Z-score with weighting factors according to the following equation:

$Z=2,213X_1+0,243X_2+0,760X_3+2,821X_4$,

where the financial ratios are as follows:

X_1 - Earnings before interest and taxes (EBIT) on total assets. This ratio has the greatest weight

X_2 - Working capital to total assets. The ratio has the lowest correlation in the function and the lowest statistical significance.

According to E. Tsvetanova, the first two financial ratios coincide with those of Altman [1], as well as their statistical significance for the model.

The next two financial ratios are structural indicators based on data from the company's statement of financial position. They largely reflect the specific factors and practices applied in the country.

X_3 - Equity to total assets. The company's equity is compared to total assets, which shows its financial stability.

X_4 - Money to total assets. A financial ratio that measures the portion of assets held in cash and cash equivalents. It is second in importance after EBIT to total assets.

The results obtained in an empirical way by E. Tsvetanova show that at values of Z-score:

Z < 0.4 - the probability of bankruptcy is very high;

Z - between 0.4 and 1.5 - companies fall into the zone of medium high probability of bankruptcy;

Z > 1.5 - there is a very low probability of bankruptcy [16].

The report assesses the company's bankruptcy risk using a Z-score. For this purpose, values of the indicators X_1, X_2, X_3 and X_4 of the company were calculated on the basis of real data for 2018 and 2019. The weighting coefficients proposed by E. Tsvetanova [16] are applied (Table 4).

Table 4. Indicators for calculating the Z-score

Indicator	Values		Z	
	2019	2018	2015	2014
X_1	0,077	0,175	0,077	0,175
X_2	0,587	0,614	0,587	0,614
X_3	0,861	0,856	0,861	0,856
X_4	0,586	0,613	0,586	0,613
Z-score			2,613	2,770

$$Z = 2,213X_1 + 0,243X_2 + 0,760X_3 + 2,821X_4 \quad (3)$$

The obtained values for Z are high - 2,613 for 2015 and 2,770 for 2018 and show that there is no risk of bankruptcy for the company.

Based on information about the financial and economic indicators of the company for the period 2011-2018, training of the neural network was performed by the method of forecasting time series [10, 11].

For each of the studied indicators - X_1, X_2, X_3 and X_4 a separate neural network is created, with 3 input parameters and one output. The information is distributed in training samples, using the "time window" method, which covers 3 consecutive years.

After the training of the neural network, at the next stage information is submitted about the indicators X_1, X_2, X_3 and X_4 for 2016, 2017 and 2018 and as a result a forecast for 2019 is obtained.

With the indicators obtained from the forecast, Z is calculated for 2019 and the value is compared with the value of Z = 2,613 for 2019, which is a result of the calculation with real data. The actual and obtained from the forecast results and the deviation are presented in Table 5.

Table 5. Results of the forecast for 2015

Indicator	Values 2019	Forecast data - 2019	Deviation (%)
X_1	0,077	0,081	5,2
X_2	0,587	0,772	31,5
X_3	0,861	0,774	-1,10
X_4	0,586	0,509	-13,14
Z-score	2,613	2,394	-8,38

The deviation is calculated by the formula:

$$Deviation(\%) = \left(\frac{x_{forecast}}{x_{value\,2019}} \right) \times 100 - 100 \quad (2)$$

where:

$X_{forecast}$ - projected value of the indicator for 2019;

$X_{value\ 2019}$ - real value of the indicator for 2019

The data for the indicator Z-score is calculated with real data for 2018 and 2019 and the data forecast by the neural network for 2019 show that for the company for both studied periods there is a very low risk of bankruptcy - the value of The Z-score is well above 1.5.

For 2019, there is a decrease in the value of the indicator X_1 - about 2 times, which is mainly due to a decrease in profit - more than 2 times for the studied periods. The values of Z-score for the two periods differ minimum limits - the deviation is -8.38%, which shows that the method of forecasting with neural networks with a "time window" - 2,968 for 2018 and 2,613 for 2019 can is used to make forecasts for future periods.

CONCLUSION

The application of neural networks and the Z-score model could serve as additional tools for forecasting and analyzing the financial indicators and the risk of bankruptcy of companies in order to assist management in drawing up plans and decisions for future development.

The study demonstrated the applicability of a neural network simulated with a "time window" to predict financial ratios. The application of the Z-SCORE model for assessing the risk of insolvency of a functioning company by means of the forecasted values of the indicators and with weighting coefficients proposed for Bulgarian enterprises has been tested.

The obtained predicted values of the indicators show high accuracy (compared to the real indicators) and the possibility to apply a neural network structure with a "time window" in order to forecast the financial indicators for future periods. On this basis, it is possible to make timely and adequate decisions by the company's management.

The obtained results outline as a direction for future research in the field of forecasting indicators for financial and economic analysis, creating more accurate and complete forecasting models - based on neural networks, by studying and simulating other structures of neural networks and / or other modeling approaches and methods.

REFERENCE

[1] Altman E., Financial Ratios, Discriminant Analysis and the Prediction of Corporate Bankruptcy, Journal of Finance,09/1968, pp. 589-609.

[2] Simeonov O., N. Petrova, Controlling, basics of controlling, operational controlling, strategic controlling, Publishing Complex - UNWE, Sofia, 2012, pp. 191.

[3] Kasarova V., The New Metrics of Corporate Financial Success, Ed. Evdemonia Production EOOD, Sofia, pp. 24.

[4] Hristov I., Integrated model for evaluation of the activity of the enterprise, "Isvestia" - Publication of the University of Economics - Varna, pp. 66-77

[5] Kasarova V., Models and indicators for analysis of the financial stability of the company. Scientific electronic archive of NBU. http://eprints.nbu.bg/637/1/FU_1_FINAL.pdf

[6] Popchev I., Lectures in Computer Science and Technology - IICT-BAS, №1, 2016, Six topics in risk management, http://parallel.bas.bg/lcst/

[7] Deneva I., Annual Activity Report - Intersection of Science and Business in the Financial Statements, Department of Accounting and Analysis, Faculty of Finance and Accounting at UNWE, pp. 8-9

[8] Chabaan A., Y. Malevergne, J. Laurent, F. Turpin, Alternative risk measures for alternative investments, AFFI 2003, pp. 9-21

[9] Kabaivanov St., Improving the accuracy of financial analysis with the help of neural networks, Reports from a scientific conference with international participation, Advanced scientific tools in management, 19. 09. 2008 - 23. 09. 2008, Ravda, Volume 1/2010 ISSN 1314-0582, pp. 247-253

[10] Laptev N., J. Yosinski, Li Erran, Li Slawek Smyl, Time-series Extreme Event Forecasting with Neural Networks at Uber, ICML 2017, Time Series Workshop, Sydney, Australia

[11] Borovykh A., S. Bohte, W.Cornelis, W. Oosterlee, Conditional Time Series Forecasting with Convolutional Neural Networks, Cornell University

[12] Chatfield C., The analysis of time series: an introduction, 2016

[13] Tsvetanova E., Adaptation of the Altman model for assessment of the risk of corporate bankruptcy for the Bulgarian conditions, Abstract of the dissertation, NBU-Sofia, 2017

[14] Popov D., Review of Altman's model for assessing the viability of small and medium enterprises, "Business Directions" magazine issue 2/2018

[15] Avelova D., A. Marchev, Jr. A. Marchev, Application of Z-SCORE model in business analysis, Advanced scientific tools in management, UNWE, cat. Management, Volume 1 (6) 2013, p. 261

[16] Tsvetanova E., Bankruptcy risk forecasting with a model based on discriminant analysis, adapted to the Bulgarian conditions, Godishnik of the Department of Administration and Management, NBU - Sofia, 2017

Decarbonizing Russia: leapfrogging from fossil fuel to hydrogen

Vladimir Potashnikov[1], Alexander Golub[1], Michael Brody[1], Oleg Lugovoy[1]
Russian Presidential Academy of the National Economy and Public Administration; potashnikov@ranepa.ru (V.P.); golub-a@ranepa.ru (A.G.); brody-m@ranepa.ru (M.B.); olugovoy@ranepa.ru (O.L.) [1]
Golub A. and Potashnikov V. carried out research for this article with the support of the Russian Science Foundation, project No. 21-18-00126

Abstract: *We examine a different approach to complete decarbonization of the Russian economy, in a world where climate policy is increasingly requiring radical reduction of emissions wherever possible. We propose an energy system that can supply solar, and wind generated electricity to fulfill all demand and which accounts for intermittency problems. This is instead of a more usual approach of planning for expensive carbon capture and storage, and a massive increase in energy efficiency and therefore a drastic reduction in energy use per unit Gross Domestic Product (GDP). Coupled with this massive increase in alternative energy, we also propose using excess electricity to generate green hydrogen. Hydrogen is a known technology that can function as storage for future electricity needs or for potential fuel use. Importantly, green hydrogen can be used as a re-placement export for Russia's current fossil fuel exports and will likely provide higher revenues. The analysis was carried out using the highly detailed modeling framework, the High-Resolution Renewable Energy System for Russia (HIRES-RUS) representative energy system. The modeling showed that there are a number of feasible combinations of wind and solar power generation coupled with green hydrogen production to achieve 100% decarbonization of the Russian economy.*
Keywords*: DECARBONIZATION, 100% RENEWABLE ENERGY, REPRESENTATIVE ENERGY SYSTEM, GREEN HYDROGEN*

1. Introduction

Global climate policy is aimed at reducing GHG, which requires radical reduction of emissions wherever possible. The replacement of primary energy sources with solar and wind, followed by hydrogen generation, is one of the possible options. This paper analyzes this possibility on the example of Russia. A highly detailed model of a representative energy system was used in the work (365day*24*hour*500 region of generations) based on real weather data. The energy system should meet twice the final demand, with constant energy exports, but with the replacement of hydrocarbons with hydrogen. A sensitivity analysis was conducted to assess the feasibility and cost of implementing such a scenario.

2. Methods

We carry out a numerical experiment that constructs a carbon-free energy system scenario. We assume that solar and wind power will provide all the primary energy consumption, some of which will be converted into hydrogen by electrolysis. Figure 1 shows the supply curve of solar and wind power versus 10 times the final energy consumption of all energy in Russia. It follows that the supply is sufficient to meet the demand with a significant availability factor, and consequently at a low price. However, the intermittency of solar and wind power, and the possible remoteness of sources from the point of consumption, can significantly increase costs.

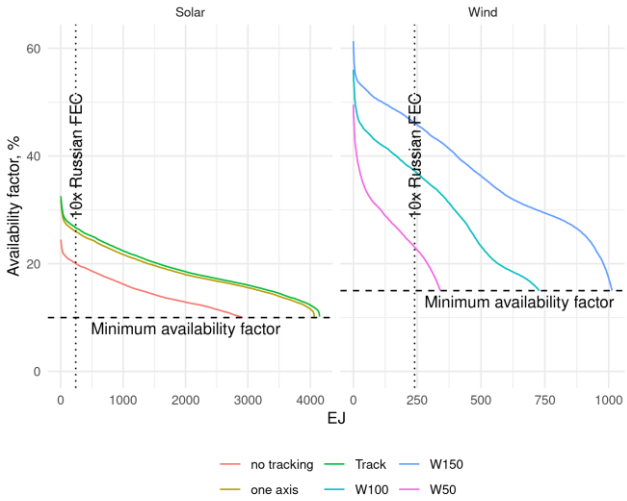


Fig. 1 *Supply curve of solar and wind electricity versus 10 times Russia's finaly energy consumption (FEC) (no more than 250 EJ)*

Russia is divided into 7 regions of a unified energy system: Center, North-West, South, Volga region, Ural, Siberia, Far East. Regions that have hard-to-reach areas (Siberia, Far East) are divided into two regions: the main one and the hard-to-reach one. In total, the RES (Representative Energy System) of Russia includes 9 regions. The model simulates one year with 365x24 time steps - into days and hours, for a total of 8,760.

To simulate intermittent energy sources, detailed weather data from NASA, the MERRA 2 project, with an hourly data and with a spatial resolution of 0.625° x 0.5°, were used. The database for Russia contains about 10,580 observations, which is beyond the numerical capabilities of modeling. For this reason, the weather data were clustered method based on data on the coordinates and hourly average profiles of generation, and average month generation. All locations for generating electricity are divided into 250 possible clusters for each type of solar and wind generation depend on its characteristics. Places where the average annual availability factors is less than 10% for solar and 15% wind were not taken into account when clustering the corresponding zones and in subsequent calculations. We also exclude location higher than 1000 m above sea level, far east places, islands and water locations. Example the clustering of data for PV with tracking systems (figure 2).

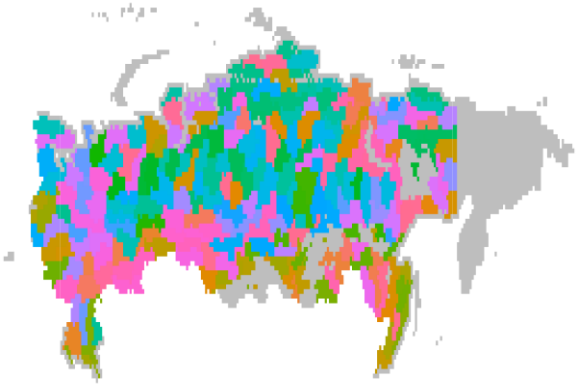


Fig. 2 *Clustering of data for PV with tracking systems*

Meteorological calibrations were from detailed data in hourly increments[1] (also see [1]). Parameters of the power generation

[1] MERRA-2 collections tavg1_2d_flx_Nx (Surface Flux Diagnostics), tavg1_2d_rad_Nx (Radiation Diagnostics), and tavg1_2d_slv_Nx (Single-level atmospheric state variables) downloaded from NASA Goddard Earth Sciences (GES) Data and Information Services Center (DISC) (https://disc.gsfc.nasa.gov/datasets?project=MERRA-2) using GNU Wget network utility (https://disc.gsfc.nasa.gov/data-access

technologies were calibrated using Lazard's Levelized Cost of Energy Analysis (Lazard), and Storage technology[2]. Key technology assumptions in the model are shown in Table 1.

Table 1. *Parameters for feasibility analysis and assumptions to achieve minimum costs, leading to 72 alternatives.*

Technology	Cost	Technical Parameter
Solar PV	Investment cost - $825/kW, Fixed Operating and Maintenance (O&M) - 9.5 $/kW/year	Solar availability factor varies between 9-28% depending on location, and is estimated using Sandia's plane-of-array model and algorithms for solar-array trackers [2] for fixed tilted, 1-axis tracking system and 2-axis tracking system, with an operational life of 20 years, and is shown in the merra2ools package3
Wind Only	Investment cost $1,050/kW, Fixed O&M - $27/kW/year	Wind availability factor can vary between 13-57% depending on station location, with precision data calculated using the merra2ools package, with an operational life of 30 years. Wind speeds for 100m and 150m were approximated from values at 10m and 50m.
Storage	$250/MWh investment cost	10% loss during charging, operational life of 15 years
500-kV HVDC bi-pole transmission line	$367M per HVDC converter station in one direction, $0.87M per 1 km, for 2.4 GW	Losses vary between 2.5% to 7.2% depending upon distance between regions (Losses = 0.6% + 2.9% for every 1000 km).
Hydrogen electrolysis	Fixed O&M, $18/kW/year, Investment cost of $900/kW/year	Efficiency of 51 kWh/kgH2, availability factor greater than 15%, with an operational life of 20 years
Hydrogen Electricity Station	Fixed O&M, $44/kW/year, with an investment cost of $700/kW	Efficiency of 65%

3. Scenario

To analyze the feasibility of 100% decarbonization of the Russian energy sector, 72 scenarios were built to assess the feasibility of the scenario to critical prerequisites. Table 2 shows the basic prerequisites for scenarios and their designation. Specific scenarios and their designations are obtained as a Cartesian multiplication of options / values. The scenarios consider three options for demand for electricity and hydrogen. In the scenario option E36, the demand for electricity is 1.5 FEC, and the demand for hydrogen is the volume of hydrocarbon exports in energy equivalent. Thus, the scenario can be interpreted as the fact that all domestic consumption goes to electricity, and hydrocarbon rent will be replaced by hydrogen. In the E12 scenario, only a third of domestic consumption goes to electricity and the rest to hydrogen. These extreme demand options show that 100% decarbonization is feasible, depending on which end-demand technologies are used. For example, will electric cars become more widespread, including in cold climates, or will hydrogen-fueled cars become more widespread. In all cases, it is assumed that for 20% of the demand for electricity, it does not matter when exactly it was produced, and consumption occurs when there is an excess of electricity, and the rest of the demand must be strictly satisfied at the time of occurrence (hereinafter hard demand).

The work does not consider the time of hydrogen electrolysis, and the hydrogen transportation system, since it can be stored for a long time and can travel long distances. Thus, replacing the demand for electricity with hydrogen is like reducing the hard part of the demand for electricity with a simultaneous increase in total demand (due to losses during the conversion of electricity to hydrogen).

Table 2. *Parameters for 2050 feasibility analysis and assumptions to achieve minimum costs, leading to 72 alternatives.*

Parameter	Alternatives	Description
Demand	1	Total electricity demand is 48 EJ, 70% is critical demand, flexible portion is 30%. Hydrogen demand is 12 EJ
	2	Total electricity demand is 24 EJ, 70% is critical demand, flexible portion is 30%. Hydrogen demand is 36 EJ
Wind	1	Wind speed at 150 m height
	2	Wind speed at 100 m height
	3	Wind speed at 50 m height
Solar	1	2-axis solar tracking
	2	1-axis solar tracking
	3	no solar tracking
Storage	1	Unlimited
	2	No more than 14 TWh (23-29% of average daily consumption)
Trade	1	Trade with full connectivity across all regions of RES
	2	Without isolated regions

The intermittency of energy sources may be one of the main fears of large-scale deployment of solar and wind energy. The solution to the problem of intermittency is possible with the help of a developed electricity transmission network and the use of energy conservation technologies. There are several types of energy conservation, each with its own advantages and disadvantages. The use of Li-ion batteries and accumulators is the most promising for large-scale networks, which can solve the problem of insufficient energy supply during the day. Despite the fundamental differences between these technologies, including the requirements for water supply, from the point of view of modeling, they are quite close. The work used Li-Ion more as the more expensive equivalent of conservation technology. If in a certain region conditions allow the creation of large-scale hydro pumped storage, then the costs of 100% decarbonization will become cheaper. The use of a solar panel tracking system, with an equal area, can increase the generation of solar panels and increase the time for generating electricity.

Figure 3 shows a comparison of capacity across the scenarios. All of these 72 scenarios are feasible and request reasonable amount of square.

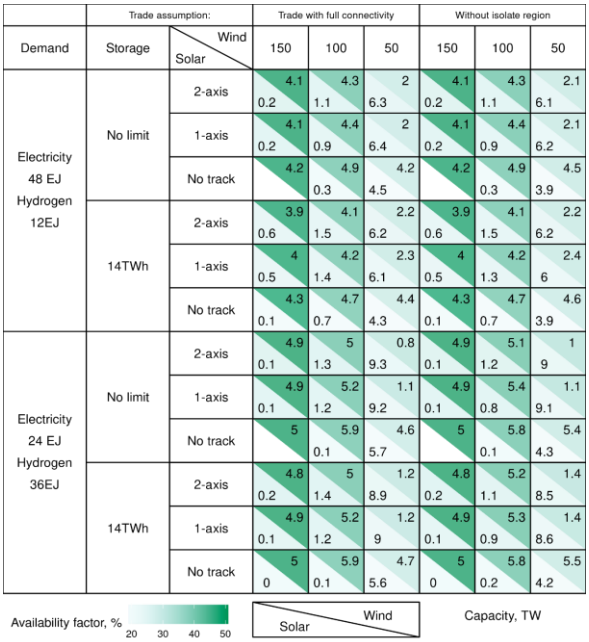


Fig. 3 *Solar and wind capacity for succeed final demands.*

[2] EA-ETSAP and IRENA© Technology Policy Brief E18 – April 2012

[3] https://github.com/energyRt/merra2ools, https://datadryad.org/stash/dataset/doi:10.5061/dryad.v41ns1rtt

Figure 4 shows the places with the highest capacity of renewable energy sources, mainly in the southern regions of the country. It is important to note the very potential high wind power in the northwest regions, although it is obvious that this region does not have significant capacity for solar energy.

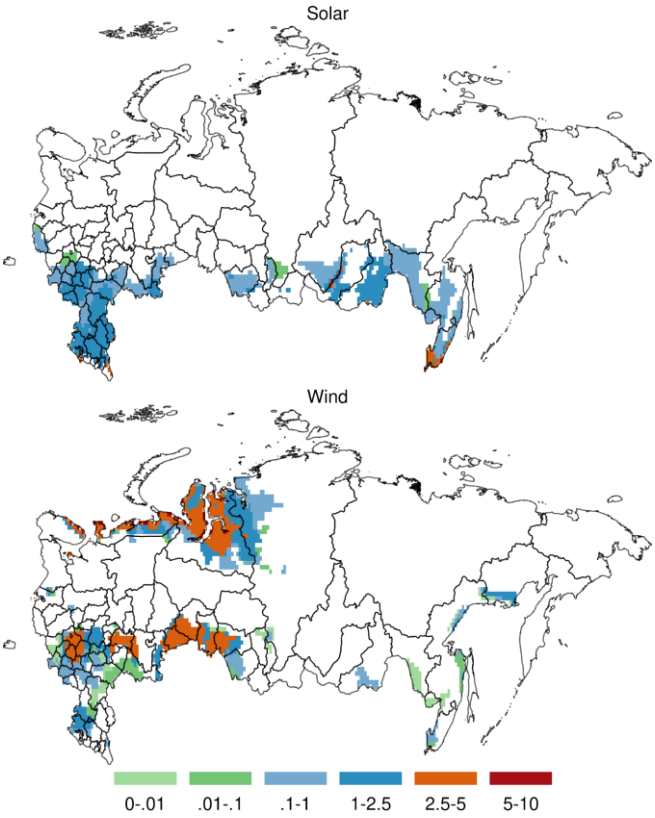


Fig. 4. *Solar and wind capacity for succeed final demands, MW per km2.*

4. *References*

1. IPCC, 2021: Summary for Policymakers. In: Climate Change 2021: The Physical Science Basis. Contribution of Working Group I to the Sixth Assessment Report of the Intergovernmental Panel on Climate Change [Masson-Delmotte, V., P. Zhai, A. Pirani, S. L. Connors, C. Péan, S. Berger, N. Caud, Y. Chen, L. Goldfarb, M. I. Gomis, M. Huang, K. Leitzell, E. Lonnoy, J.B.R. Matthews, T. K. Maycock, T. Waterfield, O. Yelekçi, R. Yu and B. Zhou (eds.)]. Cambridge University Press. In Press.
2. Sandia National Laboratories. (2021). PV Performance Modeling Collaborative. Sandia National Laboratories. https://pvpmc.sandia.gov/